Victoria, M., and A.E. Vidoz:

Tensile behavior upon ordering of Ni_3Fe single crystals.

CENTRO ATOMICO BARILOCHE
COMISION NACIONAL DE ENERGIA ATOMICA

INSTITUTO DE FISICA "Dr. J. A. BALSEIRO"
UNIVERSIDAD NACIONAL DE CUYO

SAN CARLOS DE BARILOCHE, RIO NEGRO - ARGENTINA

TENSILE BEHAVIOR UPON ORDERING OF Ni_3Fe SINGLE CRYSTALS

By

M. Victoria† and A. E. Vidoz‡

División Metales
Centro Atómico Bariloche (CNEA)
Instituto de Física
"Dr. J. A. Balseiro" (Univ. Cuyo)
San Carlos de Bariloche (R. N.)
ARGENTINA.

---

† Now at University of California, Inorganic Materials Research Dept., Berkeley, California.

‡ Now at Lockheed Missiles & Space Co., Palo Alto, California.

LOCKHEED PALO ALTO RESEARCH LABORATORY
LOCKHEED MISSILES & SPACE COMPANY
A GROUP DIVISION OF LOCKHEED AIRCRAFT CORPORATION

ABSTRACT

The tensile properties of ordered and disordered Ni_3Fe single crystal have been investigated. Also, polycrystalline specimens have been tested to show the influence of grain size on the deformation characteristics of Ni_3Fe. Measurements have been made to determine the influence of parameters such as the initial orientation of the tensile axis of single crystals, the ordered domain size, and the test temperature on the mechanical properties of Ni_3Fe.

Tensile axis reorientation during deformation was followed with x-ray techniques. It was found that in ordered single crystals, the measured tensile axis rotation agrees well with the calculated values if one activated glide system is assumed.

The influence of secondary slip on the tensile characteristics of ordered crystals was determined by using specimens oriented for multiple glide. It is demonstrated that the work hardening rate increases with the occurrence of secondary slip.

The strain-aging phenomena shown previously in polycrystalline Ni_3Fe was found to occur also in single crystals. The nature of the observed effects in ordered Ni_3Fe is interpreted in terms of the antiphase boundary tube mechanism.

LOCKHEED PALO ALTO RESEARCH LABORATORY
LOCKHEED MISSILES & SPACE COMPANY
A GROUP DIVISION OF LOCKHEED AIRCRAFT CORPORATION

1. INTRODUCTION

Several investigations undertaken during the past few years have been devoted to the study of the mechanical properties of solid solutions which develop Long-Range Order. A review paper was published recently on the subject [1]. It was found that the yield strength of these alloys is modified substantially by ordering. The nature of this phenomenon has been analysed by Cottrell [2], Brown [3], Sumino [4], Flinn [5], Marcinkowski and Miller [6], and Davies and Stoloff [7] who have proposed different models to explain this observation. In spite of the existing controversy in the interpretation of the experimental results, there seems to be little doubt that the yield stress is modified by ordering and depends upon the domain size.

Flinn [5], Cohen and Bever [8], Marcinkowski and Miller [6], Vidoz and Borwn [9], Hordon [10], Vidoz et al. [11], Popov and Orlov [12], Kear [13,14], Daview and Stoloff [15,16], Gerzha et al. [17], have investigated the influence of ordering on the plastic deformation characteristics of different solid solutions. In all these works, it has generally been concluded that an ordered alloy work-hardens more rapidly than a disordered one.

Only a few investigations have been conducted into the plastic behavior of single crystals of ordered structures, and these studies have been restricted to Cu_3Au.

After a small initial region, ordered Cu_3Au shows a high linear work hardening with a slope of approximately $G/250$, while the disordered crystals, upon deformation, present three stages similar to the characteristic stages of pure metals [13, 14, 15, 16, 18]. It must be pointed out that the first stage corresponds to the propagation of Lüders Bands. Davies and Stoloff [16] report also on the temperature and strain

rate dependence of the flow stress and work hardening of ordered Cu_3Au single crystals. They found that the critical resolved shear stress (CRSS) is independent of the test temperature but that the work hardening rate increases with increasing the temperatures.

Several models have been proposed [5, 9, 12, 13, 14, 15, 16, 19] to explain the work hardening of ordered structures, but so far not enough evidence exists to support conclusively any one of them.

In the present work the behavior of Ni_3Fe single crystals under different ordering and test conditions has been investigated. The strain aging effect shown by Vidoz et al. [11] in polycrystalline Ni_3Fe was also found in single crystals. This effect depends critically upon both the amount of prestrain and the stage in which it is given. The experimental results are discussed and it is concluded that a modified antiphase boundary tube model can explain them satisfactorily.

2. EXPERIMENTAL PROCEDURES

The alloy used was kindly prepared for this investigation by Dr. C. Dean Starr of Wilber B. Driver Co. It was made from high purity metals by vacuum casting. The ingots were hot-rolled, homogeneized and cold-rolled into a 4 mm sheet. Chemical analysis shows a composition of 72.1 ±0.1 at. % Ni and 27.9 ±0.1 at. % Fe.

Single crystals were grown in an alumina powder-soft mold using vacuum-induction high-frequency equipment. Details of the growing process are described elsewhere [20]. The grown crystals have a cylindrical shape of about 300 mm length and 3.5 mm diameter. From each single crystal, several chemical analyses were made. It was found that, within the experimental error, the composition was

homogeneous and agrees with the one of the polycrystalline materials. X-ray orientation analyses were made at both ends of the crystals. A macro-etching – 80/20 nitric acid-hydrochloric acid solution – was also used to detect the presence of grain boundaries.

Crystals were then annealed 24 hours at 1300°C in a vacuum of better than 10^{-5} mm Hg to obtain microhomogeneity. From each single crystal four to five pieces were cut using an acid saw. Each piece was masked on both ends with asphaltic paint, baked at 70°C, and etched again to obtain a gage section of 30 mm length and 2.5 mm diameter. After specimens were again annealed in vacuum at 1300°C for 24 hours to suppress the influence of previous handling, they were carefully electropolished in an 80/20 acetic acid-perchloric acid electrolite.

Tensile specimens were then ready for the special disordering or ordering heat treatments. The disordered condition was obtained by a vacuum heat treatment of 1 hour at 800°C, followed by rapid quenching into water. For ordering, the specimens, quenched as before, were annealed at 480°C in a vacuum better than 10^{-5} mm Hg for different periods of time. The specimens were then ready to be used in tensile tests. The 480°C temperature was selected to facilitate comparison of our results with the data of Davies and Stoloff [7] on the domain size of this alloy and also with the results on ordering kinetics of polycrystalline Ni_3Fe [21].

Tensile deformation was carried out at a strain rate of 10^{-4} sec^{-1} in a hard tensile machine [20], within a cage which permits changes in test temperatures. Liquid nitrogen and solid acetone baths were used for subatmospheric temperatures, whereas a silicon oil bath was utilized between room temperature and 200°C.

Lattice rotation was followed during deformation with the well-known X-ray Laüe back-reflection technique. Steel grips and a corresponding supporting cam were designed in such a way as to obtain the Laüe photographs, at different stages of deformation and on different regions of the specimen, without removing it from the grips.

Surface slip markings were observed at different amounts of strain as follows: the test was stopped and the specimen removed from the machine; its gage length was electropolished using a tampon with a 90/10 butyllcellusolve-percloric acid solution; it was then restrained 1% more and a replica was obtained from the gage surface.

3. EXPERIMENTAL RESULTS

3.1 The yield stress

Figure 1 shows the effect of annealing time at 480°C on the critical resolved shear stress of Ni_3Fe specimens. Single crystals used were all of the same crystallographic orientation, as indicated in the figure. Because this alloy does not shown a sharp yielding upon deformation, specimens were deformed at room temperature on tension up to 0.05% elongation to obtain the CRSS.

The plastic part of the tensile curve obtained was extrapolated back to intersect the extension of the linear elastic region. The shear stress corresponding to this intersection was taken as the CRSS for the test. For each experimental point shown in Fig. 1, one specimen was initially used, with the exception of the first for which two specimens were used. After termination of the yield point tests, the specimens were heat treated again to give to each the annealing time which corresponds to the

next selected experimental point. They were then retested for yield stress determination. This operation was repeated several times; thus, the last experimental point shown in Fig. 1 has been checked several times. The error which is indicated corresponds to the deviation from an average of those measurements. Therefore, average was calculated with two measurements for the first experimental point, three for the second, and so on.

The domain sizes obtained by Davies and Stoloff [7] for identical heat treatments are included in Fig. 1. The peak shown in the CRSS is located at a shorter annealing time; hence, a smaller domain size is indicated than the one found by these authors with hardness measurements.

All the specimens used were previously prepared for metallographic observations. In all cases, at the end of deformation, slip lines were observed which corresponded to only one activated slip system.

3.2 Strain hardening

Of all available crystallographic orientations, specimens on disordered and different ordered condition have been fully deformed in tension.

Figure 2 shows the resolved shear stress vs. shear strain curves for ordered and disordered crystals of initial orientation 17. These curves have been calculated assuming slip in only one activated system.

For the disordered case it can be seen the three stages of deformation characteristics of fcc alloy single crystals. A small initial yield point was observed although not in all cases. After it, deformation proceeds inhomogeneously by the development

of several randomly distributed and clearly visible macroscopic necks. Slip then propagates through the entire gage length by what seems to be Lüders bands (the fronts of these bands were found not as well defined as they should be). This behavior is in accordance with previous reported information on fcc alloys [13, 22, 23]; during this first stage, specimens show little or no work hardening at all.

Once slip propagation through the gage length uniformizes the cross-section, stage II gradually develops, showing a work hardening rate of approximately G/400, where G is, as usual, the shear modulus. When stage II is fully developed or eventually at its conclusion, surface slip markings show the activation of a secondary system. Stage III then begins and the microscopic observations indicate the presence of abundant cross-slip, which is a characteristic of the so-called "dynamical recovery."

The change in orientation of the tensile axis for disordered specimen 17B is shown in Fig. 3. Numbered circles correspond to strains indicated by arrows in Fig. 2. This result is typical of the deformation of disordered alloys. There is a small overshooting of the symmetry line (100)($\bar{1}$11), as observed previously in the literature for other alloys [22].

Figure 2 also shows a typical curve for the ordered crystals. It can be seen that after an initially lower slope, a linear work hardening region is developed up to high values of the strain, where, in some cases, as it does here, the slope becomes more pronounced.

Metallographic observations of the ordered specimens performed at different stages of deformation shows the fine slip pattern characteristic of ordered alloys (13,24]. No trace of secondary slip or cross-slip have been found, except at strains very near the fracture of the specimens or at their necking regions.

Tensile axis rotation during the deformation of the ordered crystals (17A) is also shown in Fig. 3. It can be seen that the tensile axis moves towards the $[10\bar{1}]$ primary slip direction, with no deviations from this path until the end of deformation is almost reached. This effect has been called a "complete overshooting of the symmetry line" [25]. The most striking case is that of specimen 14B which was deformed at liquid nitrogen temperature (see Fig. 4). Tensile axis at the end of test was found to be within 7° of the $[10\bar{1}]$ primary slip direction. This result was plotted, even though it was obtained at a necking of the specimen. It must be considered that the deformation necessary to obtain such orientation of the tensile axis is beyond the possibilities of any tensile test. However, such deformation seems to indicate that even during the necking of the specimen the activation of secondary system is very difficult. The point 3 is located at 18° from the $[\bar{1}01]$ direction and corresponds approximately to the calculated orientation assuming slip on the system $(111)[\bar{1}01]$. A full description of this effect has been reported elsewhere [25].

Special notice must be given to the results plotted in Fig. 2. Contrary to what has been previously reported concerning the deformation of ordered fcc single crystals [13, 15, 18], the work hardening rate of the ordered Ni_3Fe (approximately G/1000) is lower than that of the stage II disordered alloy. Moreover, previous investigation [11] has shown that polycrystalline Ni_3Fe (0.02 mm grain size) ordered with the same heat treatment as used for specimen 17 A (Fig. 2), presents a higher work hardening rate upon tensile deformation than does the corresponding disordered material.

With these results in mind the influence of grain boundaries was rapidly investigated. Figure 5 shows the tensile curves for a specimen with 1 mm grain size and

Fig. 6 the ones for an alloy with a bambu structure, i.e., with only one grain of approximately 2.5 mm diameter per section.

The influence of grain size on the work hardening rate of ordered Ni_3Fe can be seen in Table I. Here, the differences between the work hardening rates of ordered and disordered crystals ($A = \theta_{ord} - \theta_{disord}$) are calculated for all cases available. It can be concluded that A increases with the grain size, having the smallest (and negative value) for the single-crystalline specimen. For this case, the value of A was taken as the differences between θ_{ord} and θ_{disord} of stage II from the results of Fig. 2. The value of A is null for the case of the bambu structure. It means that in this condition both ordered and disordered specimens have equal work hardening rates.

Some of the as-grown orientations tended to produce double or multiple slip. Figure 7 shows the result of the tensile tests for specimens [24] which developed double glide. Even though their orientation was not near the symmetry line, they have shown double glide since the very beginning of tests. This was attributed to the roughness and lack of uniformity of the specimen's gage surface. Obviously, the activation of two systems produces a greater effect on the behavior of the ordered than on the disordered crystal. The work hardening rate is approximately the same for both specimens.

In Fig. 8 are plotted the results of the deformation tests of crystal 27. Here there were metallographic evidences of multiple glide, the presence of which could be also deduced from the fact that during deformation the cylindrical section of the specimens was preserved. In this case, similarly to what happens with polycrystalline material, the ordered specimens work harden more rapidly than the disordered ones.

(Evidences of this effect in Cu_3Au are discussed in [26]). The values of A (as defined before) for specimens 24 and 27 are also shown in Table I.

These results apparently indicate a considerable influence by the intersecting slip upon the work hardening rate of the ordered single crystals. However, special conditions must be met before such a type of glide can be completely developed. Furthermore, as shown in Fig. 9, even in the case where the initial orientation of the tensile axis is very near the symmetry line, no macroscopic double glide occurs and secondary slip is inhibited. In other words, a small amount of initial primary slip work-hardens the secondary systems so drastically that they are never able to develop macroscopic slip.

Tables II and III list the results of tests made with several ordered and disordered specimens. The corresponding crystallographic orientations are indicated in the stereographic projections shown below the tables.

Here, the values of λ_o and φ_o correspond to the initial orientation of the tensile axis, related to the primary slip direction $[\bar{1}01]$, and to the orientation normal to the primary slip plane (111), respectively. The temperature T(°K). The other parameters included are defined in the schematic graph shown in Fig. 10.

3.3 Strain hardening dependence on the antiphase domain size

The sluggishness of the ordering process in the Ni_3Fe alloys makes the investigation of the work hardening dependence on domain size particularly difficult. To grow reasonable domain sizes by means of isothermal annealings it is necessary to give the specimens long-time treatments in a vacuum furnace.

Figure 11 shows the results of three different heat treatments for specimens of the same indicated crystallographic orientation. It can be seen that the longer the annealing time, and hence the greater the domain size, the greater the work hardening rate of the ordered specimens. This is in accordance with previous results in Cu_3Au [10]. The antiphase domain sizes corresponding to the tests shown in Fig. 11 (obtained from the data of [7]) are as follows:

Specimen	480°C Annealing time (hr)	Antiphase domain size (Å)
25 B	72	30
25 C	500	65

As can be observed in Fig. 12, an 18-hr heat treatment at 480°C, although substantially increasing the yield stress, is not sufficient to produce the tensile curve characteristic of the ordered material. Such treatment only increases the length of the transition between stage I and II, the result of the test being similar to the one of the disordered crystal (specimen 5). When the time of annealing is increased to 36 hr, crystal 7 presents linear work-hardening behavior upon deformation, as shown by the well-ordered specimens. However, for this latter test a different crystallographic orientation was used than the one of specimen 5.

3.4 Strain hardening dependence on temperature

Figure 13 shows the result of tensile tests performed at different temperatures for Ni_3Fe single crystals of similar orientations. All these specimens were ordered together by an annealing treatment of 72 hr at 480°C. It can be seen that the higher

the test temperature, the greater the work-hardening coefficient. This kind of temperature dependence was also found for single crystalline Cu_3Au by Davies and Stoloff [16]. However, previous results of Vidoz et al. [11] indicate that polycrystalline Ni_3Fe does not show any significant work-hardening dependence on temperature (Fig. 14). Here only two different test temperatures have been used.

In Fig. 15 the tensile curves for ordered single crystals of multiple slip orientation (specimens 27) are given. As was mentioned before, under optical microscopic observations, all the specimens of this orientation show the activation of several glide systems during deformation. In this figure the results of tests at three different temperatures are plotted. It can be seen that for this particular crystallographic orientation work-hardening does not depend on the test temperature.

3.5 Strain aging of Ni_3Fe single crystals

To investigate whether aging effects similar to those found by Vidoz et al. [11] in polycrystalline material were present in the case of single crystals, several specimens were subjected to ordering treatments after an initial deformation in the disordered state. Figure 16 shows a typical result. The initial flow stress of the aged single crystals is similar to that of the initially ordered specimens, but the slope of the tensile curve is strongly dependent on the amount of prestrain. If the crystal has been deformed to a strain value in the "easy glide" region, the strain hardening coefficient of the curve obtained after annealing is identical to or slightly higher than the one for the initially ordered specimen, but in all cases lower than those corresponding to stage II of the disordered material. If, however, the prestrain reaches values into stage II, the corresponding slope increases to values higher than those corresponding

to stage II of the disordered specimens. A particularly striking case of this effect is shown in Fig. 17. Crystals 16 B and 16 C have prestrains differing only in 0,1 shear strain. But the curve corresponding to crystal 16 C, the crystal having been elongated into the beginning of stage II, has a slope 2,4 times higher.

4. DISCUSSION

4.1 The critical resolved shear stress

Investigations of the dependence of the yield stress of ordering alloys on the degree of order and domain size have been made by several authors [6, 7, 27, 28].

The results which are shown in Fig. 1 agree qualitatively with the information available in the literature, as far as the existence of a maximum of the yield stress as a function of annealing time is concerned. This maximum has been related to a critical domain size by using the data offered in the literature for equal heat treatments [7]. In this way the maximum in the CRSS was found to be at a very small domain size, approximately 16 Å, as can be seen in Fig. 1.

However, it is known that determinations of domain size and degree of order in Ni_3Fe are very difficult and subject to large errors if normal x-ray methods are used. Moreover, the data of Davies and Stoloff [7] show that the isothermal annealings at 480°C modify both the domain size and the degree of order for up to 100 hr of treatment. Because the maximum in the CRSS (see Fig. 1) was found for annealing times shorter than 100 hr where both domain size and degree of order are continuously modified, it is difficult to determine which one really affects the CRSS. This behavior of the yield stress of ordering alloys, which shows the existence of a maximum, has

been related by several authors [27, 28], to the mechanism proposed by Cottrell [29]. This model, the details of which are discussed elsewhere, predicts a maximum in the yield stress at a value of domain size which is approximately independent of the type of alloy. One of the hypotheses initially made by Cottrell in order to develop the model, is that there is perfect order inside the domains for all domain sizes.

The application of Cottrell's model has been discussed in the light of experimental observations. Marcinkowsky and Miller [6] found that in Ni_3Mn the maximum in the yield stress lies at values of domain size very far from the one predicted by Cottrell's model, i.e., 500 Å. Davies and Stoloff [7] have also criticized the application of this mechanism because, in Cu_3Au, they have found that for domain sizes of the order of 40 Å (approximately the value attained at the maximum) the degree of order does not achieve a constant value and is indeed modified substantially. As this fact is against the initial assumptions of Cottrell, these authors suggest that the mechanism should be revised. They suggest also a new strengthening mechanism, which consists of single dislocations cutting through the antiphase boundaries, contributing to the initial increase of the yield stress.

In spite of the existing controversy in the interpretation of the experimental results, there is little doubt that the yield stress is modified by ordering and that it depends also on domain size. More experimental data concerning the CRSS dependence on these two variables are needed for any further discussion on this subject.

4.2 Strain hardening

From the results shown in Figs. 2 and 4 and the compilations made in Tables I, II, and III, it can be seen that contrary to what has been observed in Cu_3Au [13, 15, 18],

the ordered Ni_3Fe single crystals present, upon deformation, a lower work hardening rate than the one of stage II of the corresponding disordered alloy. This observation is rather surprising inasmuch as polycrystalline Ni_3Fe (see Fig. 14), subjected to identical heat treatments, behaves similarly to Cu_3Au [11]; i.e., the ordered specimens show a higher work hardening than the disordered ones.

Also, from the results plotted in Figs. 7 and 8, it can be seen that in the cases in which double or multiple slip takes place during deformation, the single crystals behave differently, the ordered alloy showing a higher work hardening rate than the disordered one. This seems to be evidence of the influence of intersecting slip on the plastic behavior of ordered Ni_3Fe.

However, other reported results indicate that during the plastic deformation of ordered fcc alloys, secondary slip is negligible. Kear [13, 14], has shown that during deformation of ordered Cu_3Au the tensile axis rotates toward the primary slip direction in such a way that practically no contribution to the strain due to secondary systems can be accounted for. Also, the results shown in Figs. 3 and 4 illustrate that the tensile axis of the ordered Ni_3Fe single crystals rotates, upon deformation, as if only one slip system were activated. Moreover, after passing the symmetry line (100)(111) it continues its movement toward the primary slip direction $[\bar{1}01]$ showing a big overshooting effect, which is remarkable, especially in the case of crystal 14A in Fig. 4. In a previous paper [25], it was shown that the calculations assuming single slip agree, within the experimental error, with the observed lattice rotation up to very high values of deformation. This complete overshooting effect indicates the existence of a very strong latent hardening effect which reduces or eventually stops the contribution to the strain due to the secondary systems. It must be noticed that at the deformation indicated by point 3 of analysis 14A in Fig. 4, the stress applied on the conjugate system

is 1.8 times greater than the one acting on the primary system. That means that the hardening of the conjugate system is amazingly effective. However, in Figs. 7 and 8 the results on the deformation of double and multiple slip oriented crystals indicate that for these orientations it is possible to obtain secondary slip, whose effect is much more pronounced upon the behavior of ordered than upon disordered specimens (see Table I). Similar results have been obtained using Cu_3Au ordered single crystals [26]. From the results of the present work, we may conclude that when orientations are such that deformation starts by single glide (see Fig. 9), this drastically affects the secondary systems, producing a large, permanent latent hardening effect. However, when several slip systems can be activated initially, the deformation proceeds by multiple glide, indicating a greater work hardening coefficient for ordered crystals than for single glide orientations.

The case of the polycrystalline material is similar to the one of multiple slip orientated crystals. Here, the influence of the grain boundaries rapidly uniformizes the applied stress on all possible slip systems, giving place to deformation in several glide systems. The uniformization of the applied stress should be more rapid, the smaller the grain size of the alloy. This phenomenon offers an explanation of the dependence of the work hardening on the grain size shown in Figs. 5, 6, and 14. The observed fact that secondary slip gives an important contribution to the work hardening of the ordered alloys suggests the intersection of dislocations as the controlling mechanism for the deformation of these structures.

Several models [5, 9, 13, 14, 15, 16], have been proposed to explain the deformation characteristics of ordered solid solutions. The mechanism proposed by Flinn [5] can be eliminated from consideration in this discussion, because it needs

extensive multiple slip to account for the reduction of domain size and predicts an incorrect dependence of the work hardening upon the domain size [29].

The model introduced by Kear [13] and modified by Davies and Stoloff [16], is based on the cross-slip of superdislocations onto the cube planes of the crystal. In both papers, the influence of this cross-slip is interpreted in a different way, but no explanation is given for its existence. It seems unclear whether there is cross-slip onto the cube planes; no cross-slip has been ever observed in these ordered alloys [11, 24]. On the other hand, the disordered alloys show a profuse cross-slip [11, 24], as has already been discussed by Vidoz [30].

A model that makes use of the intersection of dislocations on different glide systems has been proposed by Vidoz and Brown [9] in which secondary slip must occur so that the dislocation in secondary systems can produce jogs and hence antiphase boundary (APB) tubes on the slipping superdislocations. However, it has been already shown by Vidoz [31], that the forest increase necessary for the applicability of the APB tube model is so small that it may not be observed experimentally.

The results discussed here indicate the influence of secondary slip on the work hardening of ordered alloys as well as the existence of a hardening of secondary systems due to initial slip on the primary system. This "latent hardening effect," which – as was already discussed – affects the plastic properties in different ways depending on the initial crystallographic orientation, does not mean the total absence of secondary glide [31]. It merely indicates that the contribution of the secondary systems to the macroscopic strain is limited and can in some cases be too small to be detected. But secondary glide, even when not macroscopically observed, can exist in a very small scale, giving rise to a forest increase which is necessary for the application of the APB tube model.

4.3 Strain hardening dependence on domain size and test temperature

It has been shown that the strain hardening of ordered solid solutions is modified by the domain size [10], being greater the greater the domain size. From the results of Fig. 11 it can be seen that the Ni_3Fe single crystals behave accordingly. However, in this case, the domain sizes obtained with reasonable isothermal annealing times are much smaller than the ones used for Cu_3Au in previous investigations [13, 14, 15, 16, 18]. Thus, we may conclude that ordered Ni_3Fe single crystals with large domain sizes, as obtained for Cu_3Au (10^{-5} cm), would show upon deformation a work hardening rate greater than the one of stage II of the disordered crystals.

That the domain size dependence cannot be explained with the model proposed by Flinn [5] has been already demonstrated by Pampillo [29] who pointed out that this model predicts an increasing of the work hardening with decreasing domain size.

The mechanism based on the cross-slip of superdislocations [13] onto the cube planes also does not offer a feasible explanation for this domain size dependence. The APB tube mechanism as introduced originally by Vidoz and Brown [9] also does not consider any dependence of the work hardening rate on temperature, domain size, or degree of order. However, these authors overlook the hardening of secondary systems, consideration of which might give place to the mentioned dependences [31].

Let us analyze the deformation process of an ordered single crystal assuming that most of the hardening is due to the APB tube creation during the intersection of superdislocations. Figure 18 (from [31]) represents schematically the resolved shear stress acting on the primary and conjugate system as a function of primary shear strain. We first discuss the case of an ordered crystal which has a small domain size and consequently a large yield stress (Fig. 18a): plastic deformation starts when the

applied resolved shear stress on the primary system reaches the critical value and primary superdislocations moving through the elastic stresses of other slipping dislocations give place to a small strain hardening, as observed experimentally (Figs. 2 and 4).

As the deformation proceeds, the stress on the primary system increases due to this effect and would eventually reach a value like the one indicated by τ_s, when the rotation of the tensile axis moves it over the symmetry line (100)(111). During this stage APB tubes are created, but as there is no increase in forest, their contribution to the flow stress is constant with the strain.

Let us assume that the initial applied stress on the conjugate system is τ_c^y (Fig. 18). At a deformation a_s corresponding to the tensile axis on the symmetry line the stresses acting on both systems must be equal. Somewhere before a_s, at a value of strain a^*, the stress applied on the conjugate system reaches the value necessary for dislocation movement (for simplicity we assume it to be τ_p^y). When this stage is reached the conditions for glide on the two systems are different: primary superdislocations on their movement intersect a forest which is approximately the growth in forest of the structure, but conjugate superdislocations find in their way a much higher forest density than the growth in the crystal. This is so because the dislocations introduced by the initial primary glide (before a*) constitute an increment to the forest seen by conjugate superdislocations. On further slip, conjugate superdislocations intersected by a greater forest acquire a greater density of APB tubes than the primary ones. Because the APB tube density is related linearly to the stress to move the dislocations and this is similar for both systems, it follows that conjugate superdislocations must move a shorter distance than primary superdislocations [31].

In this way the latent hardening effect can be explained as well as the negligible contribution of secondary slip to the macroscopic shear strain.

The primary superdislocations feel the increase in forest due to the propagation of conjugate glide. The probability of intersections increases, giving rise to the formation of a greater density of APB tubes. To maintain the deformation conditions as before a more rapid increase of the stress becomes necessary, and therefore the work hardening increases.

For large domain sizes, the critical shear stress is much smaller, and the situation changes as indicated in Fig. 18b. Using the same analysis we can easily show that for identical crystallographic orientation the activation of conjugate slip takes place in this case at a smaller value of strain a^* ; i.e., the larger the domain size the smaller is the strain a^* at which conjugate superdislocations start to move. Thus, the latent hardening of secondary systems depends on the domain size. It becomes greater, as the value of a^* increases, and hence, as the domain size of the structure is smaller. Because the contribution of conjugate slip greatly influences the work hardening rate, it follows easily that the smaller the domain size, the smaller the work hardening rate of the ordered alloy-crystals, as observed experimentally.

The temperature dependence of the work hardening rate of ordered crystals has been suggested as being due to the intersection process between primary and conjugate superdislocations [31]. Increases in test temperature increase the contribution to slip of conjugate superdislocations and hence the work hardening rate of the alloy. If this is the operating mechanism, no temperature dependence can be expected when primary and secondary systems contribute equally to the deformation. This effect has been observed for the case of specimen 27 (Fig. 15) and for polycrystalline Ni_3Fe (Fig. 14).

4.4 Strain aging

Figures 16 and 17 demonstrate that in Ni_3Fe single crystals we also find the strain aging effect reported for the polycrystalline alloy [11]. This phenomenon can be explained by the APB tube model. During the prestrain of the disordered specimen and after the initial "easy glide" region, conjugate slip takes place much more efficiently than is the case for ordered crystals. This is apparent in the movement of the tensile axis during deformation (see Fig. 3). After being annealed for ordering, the specimen will have an orientation which will permit the activation of primary and conjugate slip simultaneously (applied stresses on both systems are approximately equal). However, the difference between primary and conjugate densities is now smaller than for the case of an initially ordered crystal at the onset of conjugate slip. On retesting, the specimen should show greater activation of conjugate glide, the smaller the difference between the dislocation densities on both systems, and hence the greater the prestrain. This should be reflected in an increase in the work hardening rate as it is experimentally observed (section 4.3). When prestrain of the disordered specimen is introduced into stage I (see Fig. 10) before any activation of secondary glide, the dislocation densities on both primary and conjugate systems should be much more nearly the same as they are for the case of an initially ordered material strained to the same amount. Upon ordering and retesting, no important change of the work hardening rate with respect to that of the initially ordered material should be noticed, and this is shown to occur in the results represented in Figs. 16 and 17. The low yield stress values of the prestrained and ordered specimens may be associated with an annihilation of dislocations during the ordering treatment which should affect the absolute value of the flow stress.

5. CONCLUSIONS

It has been determined that the critical resolved shear stress of Ni_3Fe single crystals changes upon ordering treatment, showing the existence of a maximum treatment of approximately 50 hr at 480°C. Similar to other ordering alloys, it is suggested this behavior corresponds to the coarsening of the domain size upon annealing.

As opposed to Cu_3Au, the work hardening rate of ordered Ni_3Fe single crystals is smaller than that of stage II of the disordered specimens. This effect is attributed to the small domain size obtained in Ni_3Fe, even after very long heat treatments for ordering. As in Cu_3Au, the work hardening rate is modified by the annealing time for ordering, with longer times resulting in greater measured work hardening rate. Increasing the test temperature results in an increase of the work hardening rate. This effect is, however, much smaller than for the case of ordered Cu_3Au single crystals.

The influence of secondary slip increases the work hardening rate. However, secondary glide activation is critically dependent upon the crystallographic orientation of the specimen with respect to the tensile axis. For orientation which favors primary glide, secondary slip is always very small and the specimens show a low work hardening rate. This rate markedly increases when the tensile axis rests initially on a double or multiple slip orientation. Upon deformation, a large tensile axis overshooting of the symmetry line was observed. This effect is interpreted as a hardening of secondary systems produced by the initial primary glide. Finally, strain aging effects, as reported previously in polycrystalline Ni_3Fe, have been observed in single crystals of this alloy.

The experimental results are discussed mainly in connection with the antiphase boundary tube mechanism, and it is concluded that this model accounts qualitatively for most of the observed experimental effects.

Acknowledgments

The authors acknowledge the assistance of Messrs. M. A. Audero and R. Runge. This work was partially supported by the U. S. Army Research Office.

REFERENCES

1. N. S. Stoloff and R. G. Davies, Progress of Materials Sciences, B. Chalmers, ed., Pergamon Press, Vol. 13(1) (1966)

2. A. H. Cottrell, Relation of Properties to Microstructure, ASM Seminar, p. 131 (1953)

3. N. Brown, Mechanical Properties of Intermetallic Compounds, J. H. Westbrook, ed., John Wiley & Sons, p. 177 (1960)

4. K. Sumino, Scientific Reports of the Research Institute, Tohoku University, Japan, Vol. 10, p. 283 (1958)

5. P. A. Flinn, trans. AIME, Vol. 218, p. 145 (1960)

6. M. J. Marcinkowski and D. S. Miller, Phil. Mag., Vol. 6, p. 871 (1961)

7. R. G. Davies and N. S. Stoloff, Act. Met., Vol. 11, p. 1347 (1963)

8. J. B. Cohen and M. B. Bever, trans. AIME, Vol. 218, p. 155 (1960)

9. A. E. Vidoz and L. M. Brown, Phil. Mag., Vol. 7, p. 1167 (1962)

10. M. J. Hordon, trans. AIME, Vol. 227, p. 260 (1963)

11. A. E. Vidoz, D. P. Lazarevie, and R. W. Cahn, Act. Met., Vol. 11, p. 17 (1963)

12. L. I. Vasilyev and A. N. Orlov, Phys. Met. and Metallography, Vol. 15, No. 4, p. 1 (1963)

13. B. H. Kear, Act. Met., Vol. 12, p. 555 (1964)

14. B. H. Kear, Act. Met., Vol. 14, p. 659 (1966)

15. R. G. Davies and N. S. Stoloff, Phil. Mag., Vol. 29, p. 349 (1964)

16. R. G. Davies and N. S. Stoloff, Phil. Mag., Vol. 12, p. 297 (1965)

17. L. A. Gerzha, V. I. Syntkina, and E. S. Yakovleva, Fiz. Met. Metallored, Vol. 18, p. 770 (1964)

18. G. Sachs and J. Weerts, Z. Phys., Vol. 67, p. 507 (1931)

19. E. V. Kozlov and L. E. Popov, Soviet Phys. Doklady, Vol. 8, p. 928 (1964)

20. M. P. Victoria, Ph.D. Thesis, Inst. de Fisica, "Dr. J. A. Balseiro," Univ. Cuyo, S. C. de Bariloche (RN) Argentina (1966)

21. C. F. Varotto and A. E. Vidoz, to be published

22. T. E. Mitchell and P. R. Thornton, Phil. Mag., Vol. 8, p. 1127 (1963)

23. G. R. Piercy, R. W. Cahn, and A. H. Cottrell, Act. Met., Vol. 3, p. 331 (1955)

24. T. Taoka, K. Yasukochi, and R. Honda, Mechanical Properties of Intermetallic Compounds, J. H. Westbrook, ed., John Wiley & Sons, p. 192 (1960)

25. M. P. Victoria and A. E. Vidoz, Act. Met., Vol. 15, p. 676 (1967)

26. M. P. Victoria, M. A. Audero, and A. E. Vidoz, to be published

27. W. D. Biggs and T. Broom, Phil. Mag., Vol. 45, p. 246 (1954)

28. G. W. Ardley, Act. Met., Vol. 3, p. 525 (1955)

29. C. A. Pampillo, Phil. Mag., Vol. 124, p. 693 (1966)

30. A. E. Vidoz, Act. Met., Vol. 10, p. 1099 (1965)

31. A. E. Vidoz, accompanying paper

FIGURE CAPTIONS

Figure 1 Effect of annealing time at 480°C on the critical resolved shear stress of Ni_3Fe.

Figure 2 Resolved shear stress vs. shear strain curves for ordered and disordered Ni_3Fe crystals.

Figure 3 Change in orientation of the tensile axis during deformation of ordered (17A) and disordered (17B) Ni_3Fe single crystals. Numbered circles correspond to shear strains indicated by arrows in Fig. 2.

Figure 4 Resolved shear stress vs. shear strain curves for ordered Ni_3Fe crystal deformed at 77°K (14B) and 290°K (14A). The corresponding change in orientation of the tensile axis is also shown.

Figure 5 Tensile curve for polycrystalline ordered (2) and disordered (1) Ni_3Fe. Average grain size 1 mm.

Figure 6 Tensile curve for ordered (2) and disordered (1) Ni_3Fe with a bamboo structure (one grain size per cross section of approximately diameter 2.5 mm).

Figure 7 Tensile curve for ordered (24B) and disordered (24A) single crystals which show double glide.

Figure 8 Tensile curve for ordered (27B) and disordered (27A) Ni_3Fe single crystal of multiple glide orientation.

Figure 9 Resolved shear stress vs. shear strain curves for Ni_3Fe single crystals with tensile axis orientation near the symmetry line (001) ($\bar{1}11$). Ordered specimens have been deformed at 80°K (13A) and 293°K (13B) and disordered crystal at 80°K (13C).

Figure 10 Schematic representation of resolved shear stress vs. shear strain for the case of ordered and disordered crystals.

Figure 11 Tensile curves for Ni_3Fe single crystals indicating the influence of ordering annealing treatment.

Figure 12 Resolved shear stress vs. shear strain curves for Ni_3Fe single crystals of two orientations showing effect of annealing time for ordering.

Figure 13 Resolved shear stress vs. shear strain curves for Ni_3Fe single crystals showing the effect of test temperature.

Figure 14 Tensile curves for polycrystalline ordered and disordered, Ni_3Fe deformed at 80 and 293°K (average grain size 0.02 mm).

Figure 15 Tensile curve of Ni_3Fe single crystals of multiple slip orientation deformed at 80, 293, and 473°K.

Figure 16 Resolved shear stress vs. shear strain curves for Ni_3Fe single crystals showing strain aging effects.

Figure 17 Resolved shear stress vs. shear strain curves for Ni_3Fe single crystals showing strain aging effects.

Figure 18 Schematic representation of the resolved shear stress acting on the primary and conjugate systems vs. primary shear strain.

TABLE TITLES

Table I. Work hardening rates of ordered (θ_{ord}) and disordered (θ_{disord}) specimens and their difference ($A = \theta_{ord} - \theta_{disord}$) for differently oriented single crystal and polycrystalline Ni_3Fe of different grain size.

Table II. Crystallographic orientation and data on the deformation characteristics of disordered Ni_3Fe single crystals. Parameters are defined in Figure 10.

Table III. Idem as Table II for ordered Ni_3Fe single crystals.

Table I

Specimen	kg/mm^2			Grain Size
	θ_{disord}	θ_{ord}	A	
Polycrystal (Fig. 14)	170	260	90	0.01
Polycrystal (Fig. 5)	100	141	41	1 mm
Polycrystal (Fig. 6)	92	92	0	2.5 mm
Single Crystal 27 (Fig. 8)	105	151	46	–
Single Crystal 24 (Fig. 7)	106	106	0	–
Single Crystal 17 (Fig. 2)	22.2	5.9	-16.3	–

CRYSTAL	λ_o	φ_o	T(°K)	(τ_o kg/mm2)	τ_{II}	τ'_{II}	τ_{III}	ϵ'_{II}	ϵ_{II}	ϵ_{III}	(θ_I kg/mm2)	θ_{II}
L5	41°	60°	293°	3,3	3,46	3,56	13,61	0,455	0,295	0.989	0.73	19,1
L7	45°	47°		3,15	3,7	3,95		0,5	0,395		1,51	13,67
L8	36°	55°		3,20	3,55	3,70	9,60	0,397	0,27	0,835	1	13,6
L10	36° 30'	55°30'		3,50	3,6	3,70		0.368	0,216		0.58	13,3
L12	41°	56°30'		3,05	3,9	41	10,3	0,510	0,425	0,915	3,3	15,4
L16	43°	51°30'		3,35	3,50	3,55	11,8	0,345	0,295	0,855	1	16,1
L17	43°	47°30		3,30	4,15	4,6	1,4	0,480	0,352	0,905	3,3	22,2
L20	42°	48°		3,40	3,85	39	11,9	0,540	0,465	1,0	1	17,4
L9	37°	56°30'	473°	2.55	2,60	2,61	7,65	0,467	0,36	0,92	~0	10,5
L13	35°	54°	80°	5,3	6,8	7,85	13,35	0,425	0,260	0,660	6,4	23,8
L14	37°	59°		5,1	5,35	5,50	11,9	0,625	0,420	0,910	0,8	22,8

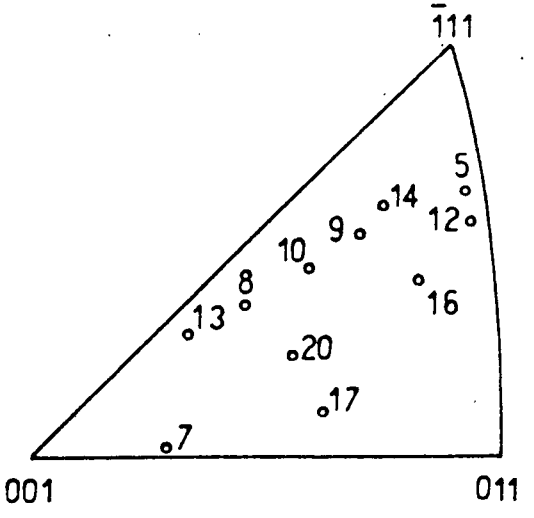

Table II

CRYSTAL	λ_o	φ_o	T(°K)	ANNEALING TIME (480°C)	τ_o (kg/mm²)	$\Theta_{ord.}$ kg/.mm2	Θ_o	ϵ_o
L5	41	60	293°	120 HRS.	4,9	9	5,3	0.359
L7	45	47	293°	36 "	5,3	5,8	4,6	0,25
L7				108 "	4,5	8,1	6,1	0,32
L8	36	55		120 "	4,75	5,8	3,9	0,37
L10	36°30'	55°30'		72 "	5,7	7,4	5,8	0,445
L12	41	56°30'		72 "	4,8	7,3	3,7	0,375
L13	35	54°		72 "	5,35	12,0	8	0,345
L14	37	59°		72 "	6,25	6,5	4,9	0,275
L16	43	51°30'		72 "	5,15	11,21	5,1	0,270
L17	47°30'	43		72 "	5,65	5,9	4,2	0,290
L20	42	48°		72 "	5,9	7,1	5,5	0,250
L9	37	56°30'	473°	72 "	3,8	7,3		
L13	35°	54°	80°	72 "	7,5	11,2	3,6	0,195
L14	37°	59°		72 "	7,1	5,8	3,7	0,255

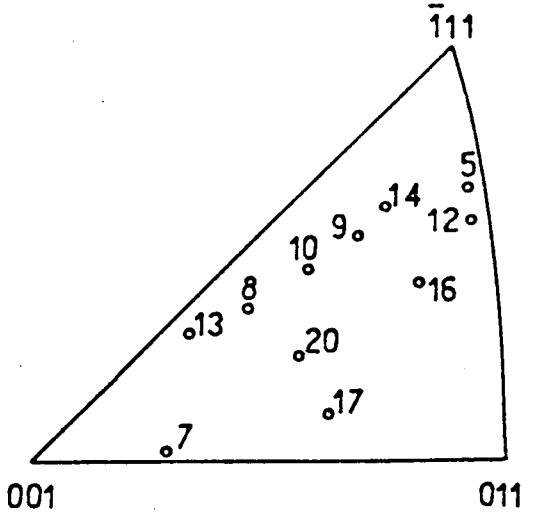

table III

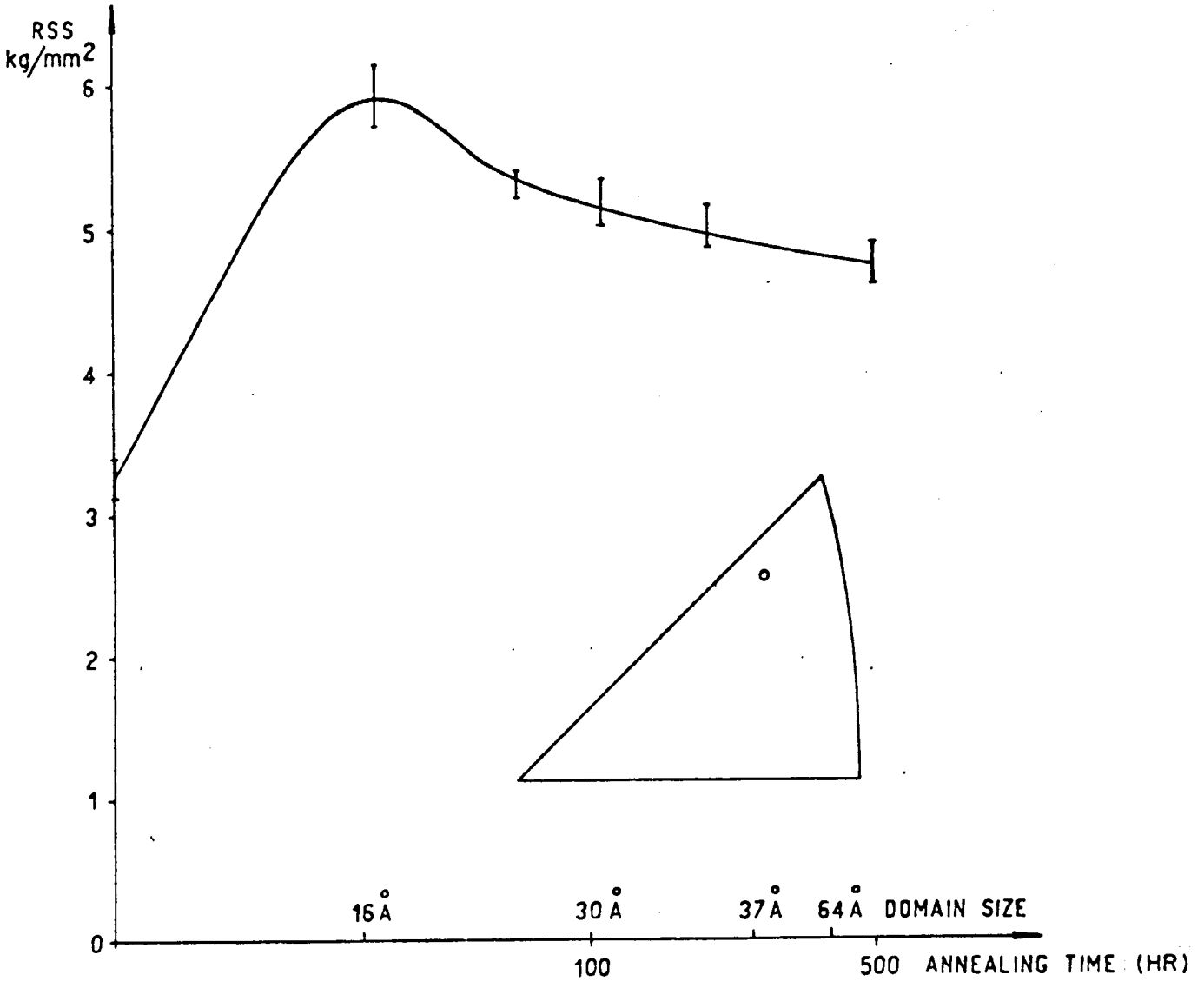
RSS
kg/mm2
6
5
4
3
2
1
0
16 Å
30 Å
37 Å
64 Å
DOMAIN SIZE
100
500
ANNEALING TIME (HR)

Figure 1

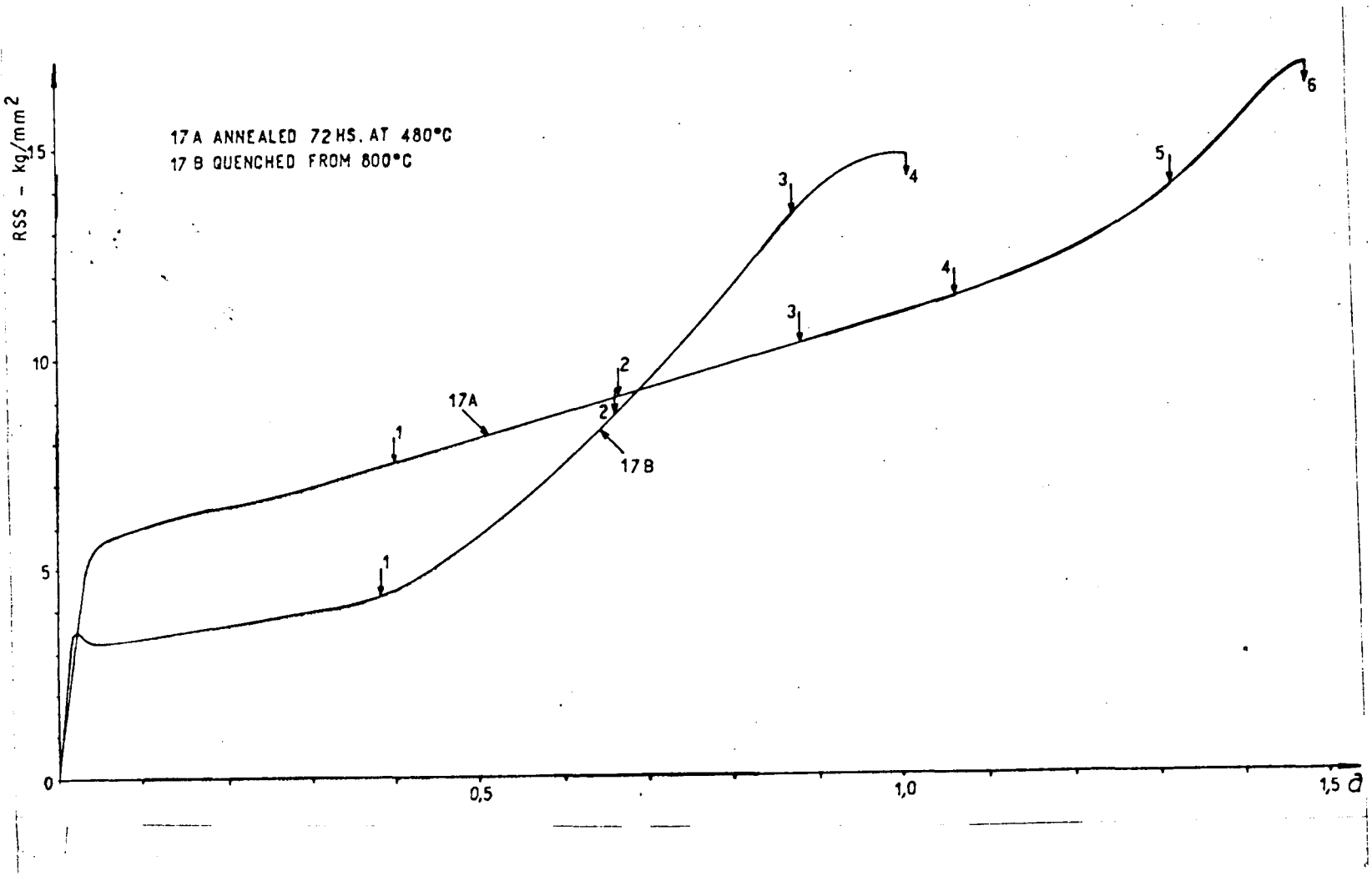
17 A ANNEALED 72 HS. AT 480°C
17 B QUENCHED FROM 800°C
RSS - kg/mm²
15
10
5
0
0,5
1,0
1,5 d
17A
17B
1
2
3
4
5
6

Figure 2

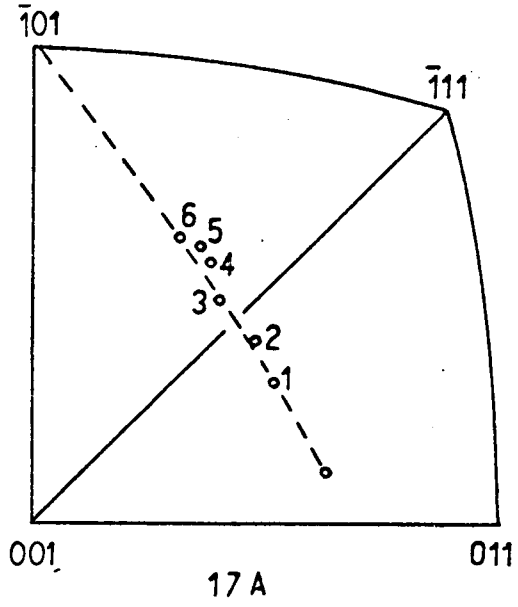

17 A

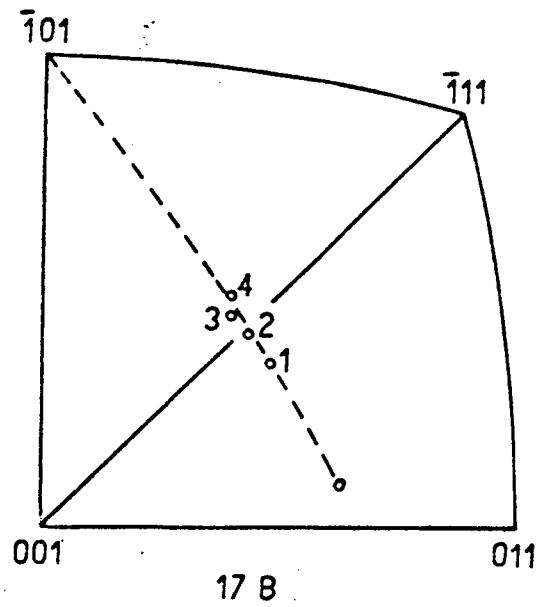

17 B

Figure 3.

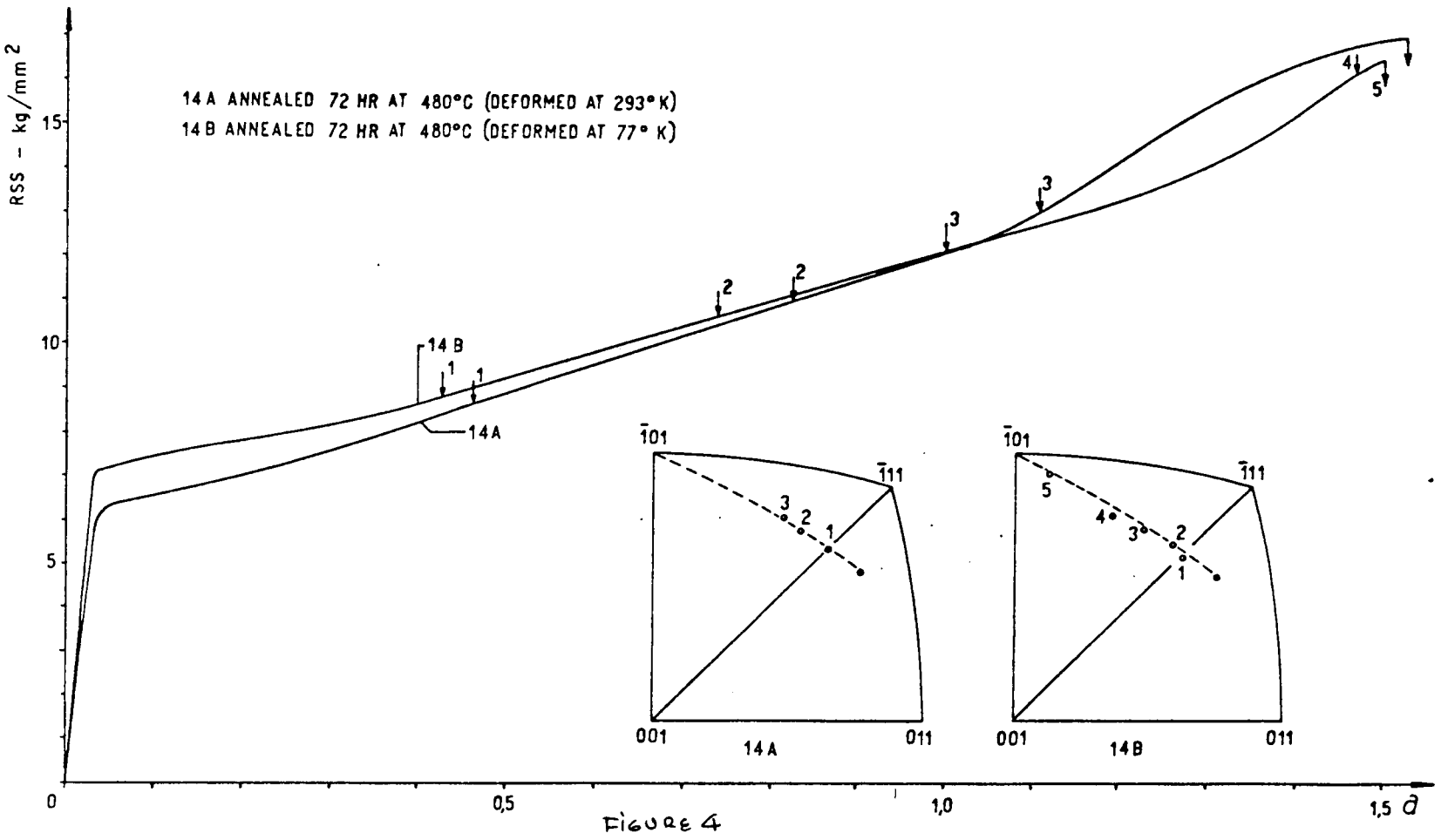
14 A ANNEALED 72 HR AT 480°C (DEFORMED AT 293° K)
14 B ANNEALED 72 HR AT 480°C (DEFORMED AT 77° K)
RSS - kg/mm 2
15
10
5
0
0,5
1,0
1,5 d
14 B
14 A
1
2
3
4
5
$\bar{1}01$
$\bar{1}11$
001
011
14 A
14 B

Figure 4

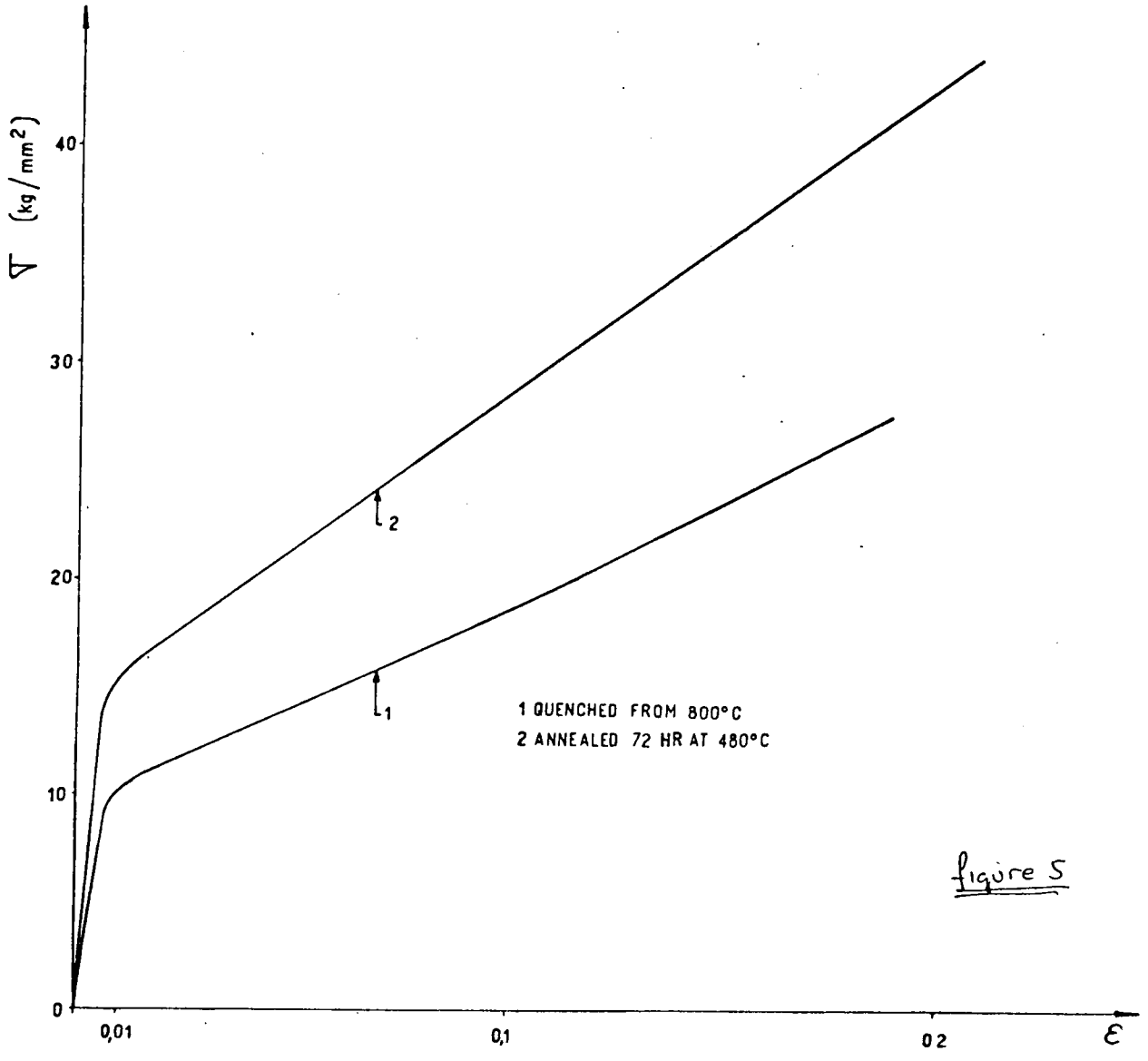
σ (kg/mm²)
40
30
20
10
0
0,01
0,1
0 2
ε
2
1
1 QUENCHED FROM 800°C
2 ANNEALED 72 HR AT 480°C

figure 5

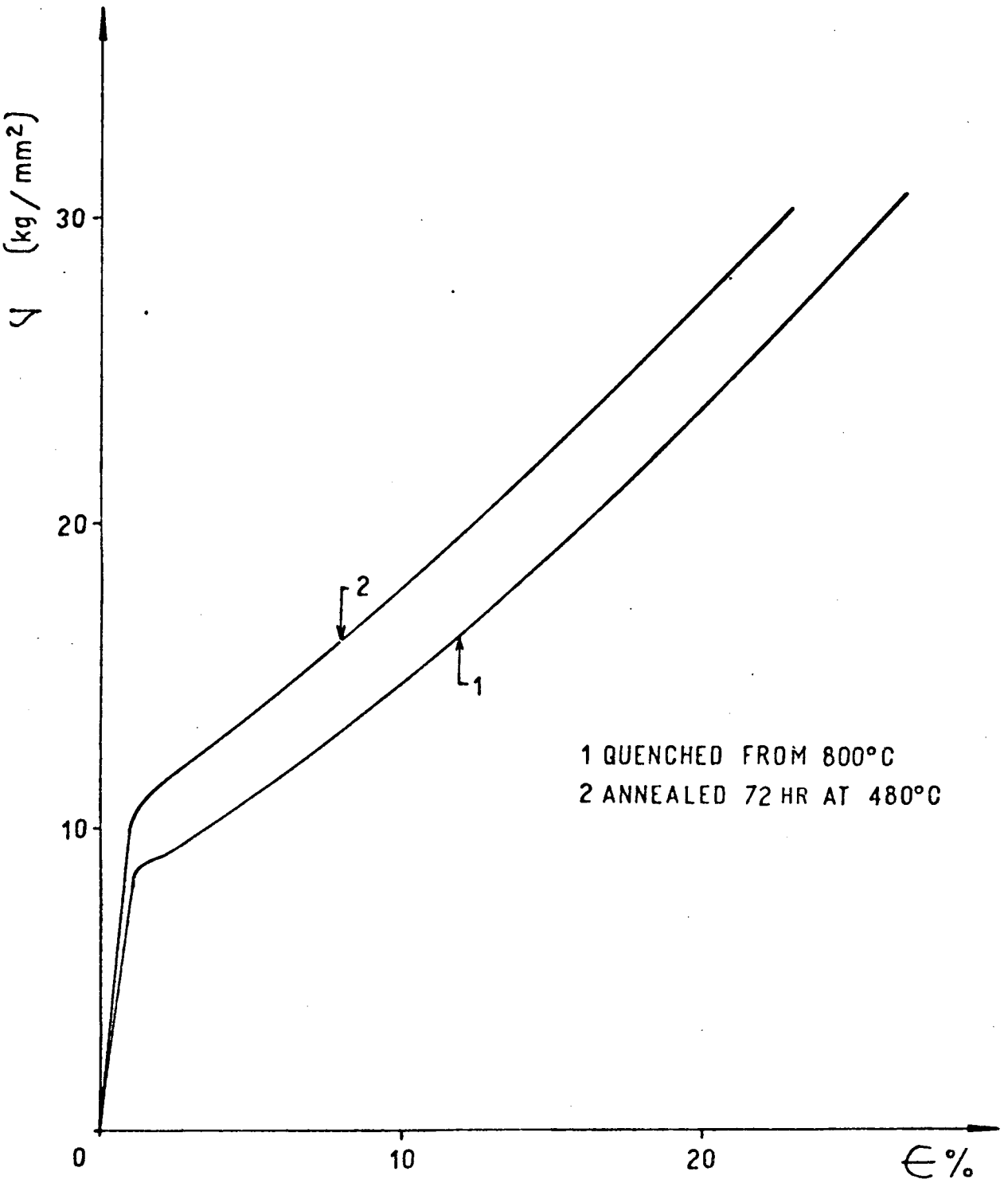
σ (kg / mm²)
30
20
10
0
10
20
ε %
2
1
1 QUENCHED FROM 800°C
2 ANNEALED 72 HR AT 480°C

Figure 6

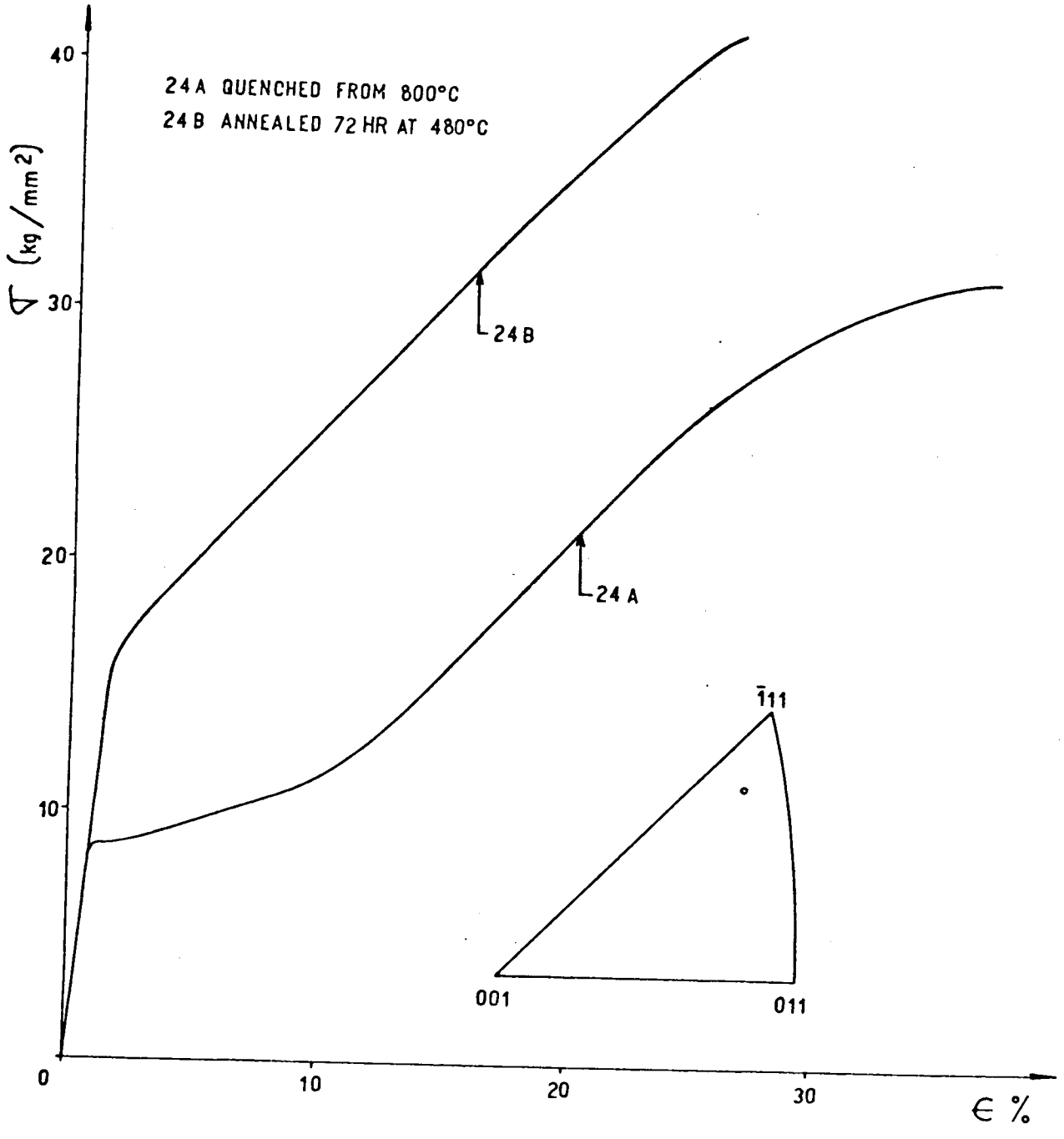
24 A QUENCHED FROM 800°C
24 B ANNEALED 72 HR AT 480°C
σ (kg/mm²)
40
30
20
10
0
24 B
24 A
$\bar{1}11$
001
011
10
20
30
ε %

Figure 7

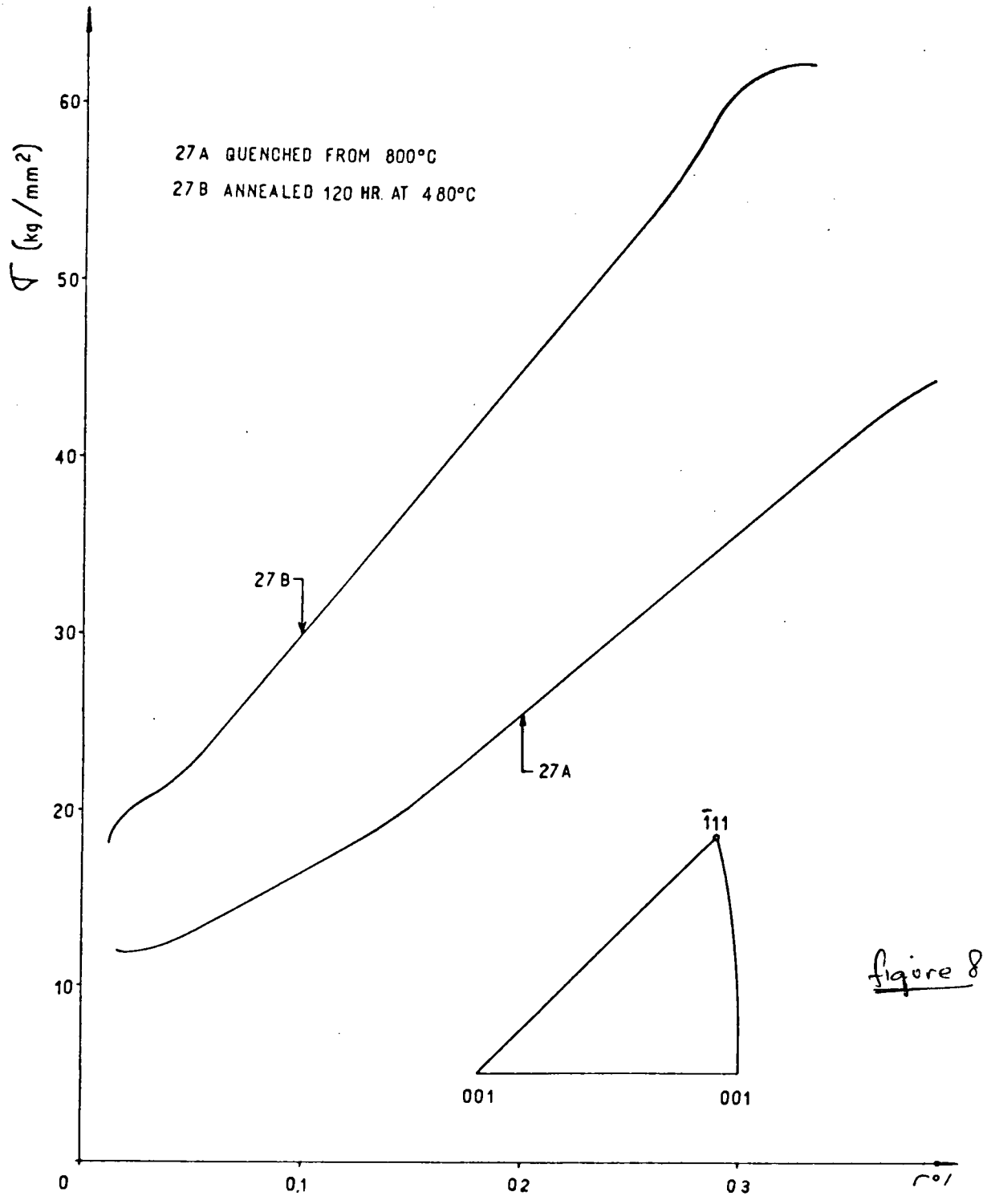
27A QUENCHED FROM 800°C
27B ANNEALED 120 HR. AT 480°C
σ (kg/mm²)
60
50
40
30
20
10
0
0,1
0,2
0,3
ε%
27B
27A
$\bar{1}11$
001
001

figure 8

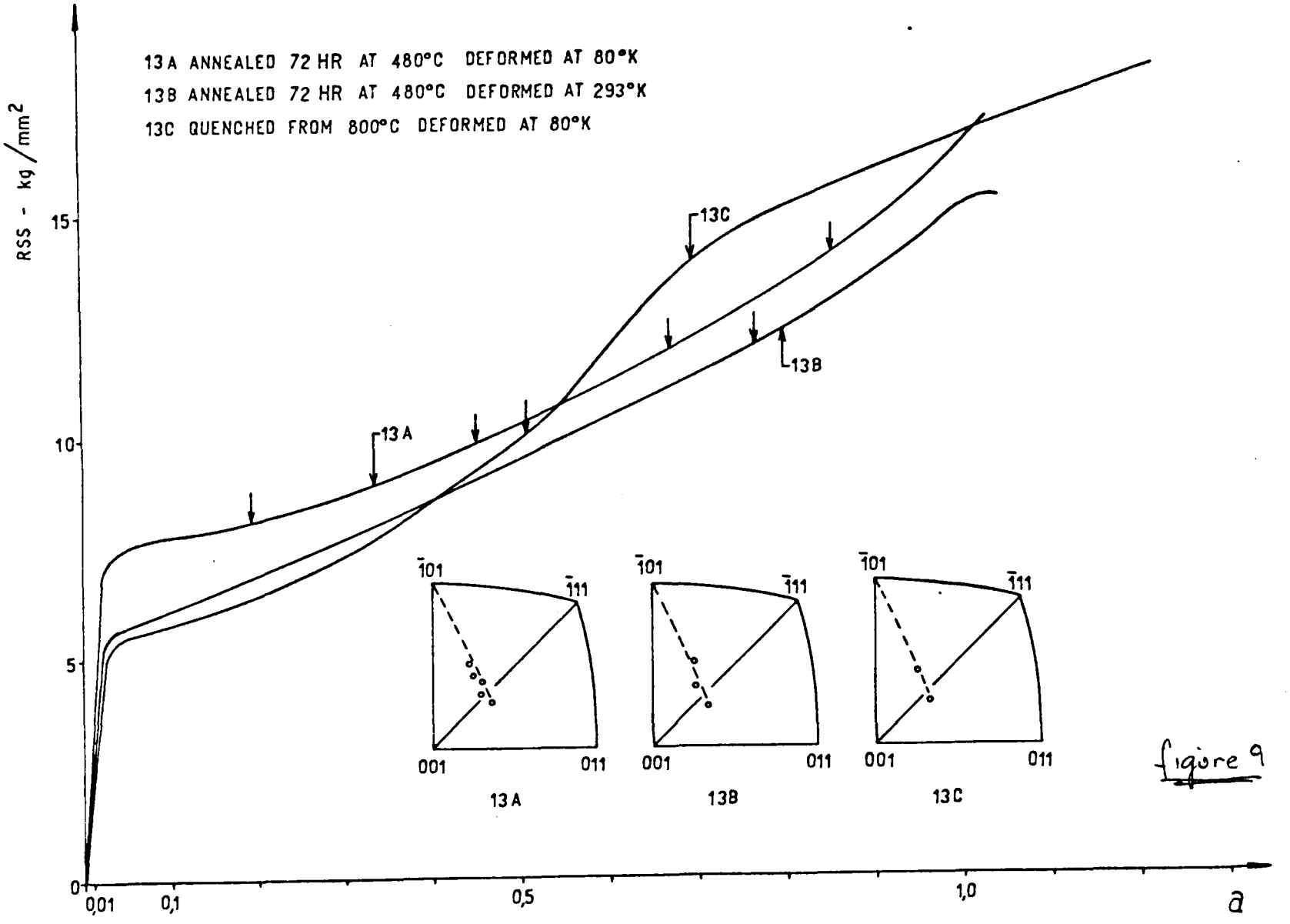
13A ANNEALED 72 HR AT 480°C DEFORMED AT 80°K
13B ANNEALED 72 HR AT 480°C DEFORMED AT 293°K
13C QUENCHED FROM 800°C DEFORMED AT 80°K
RSS - kg/mm²
15
10
5
0
0,01
0,1
0,5
1,0
a
13C
13B
13A
$\bar{1}01$
$\bar{1}11$
001
011
13A
13B
13C

figure 9

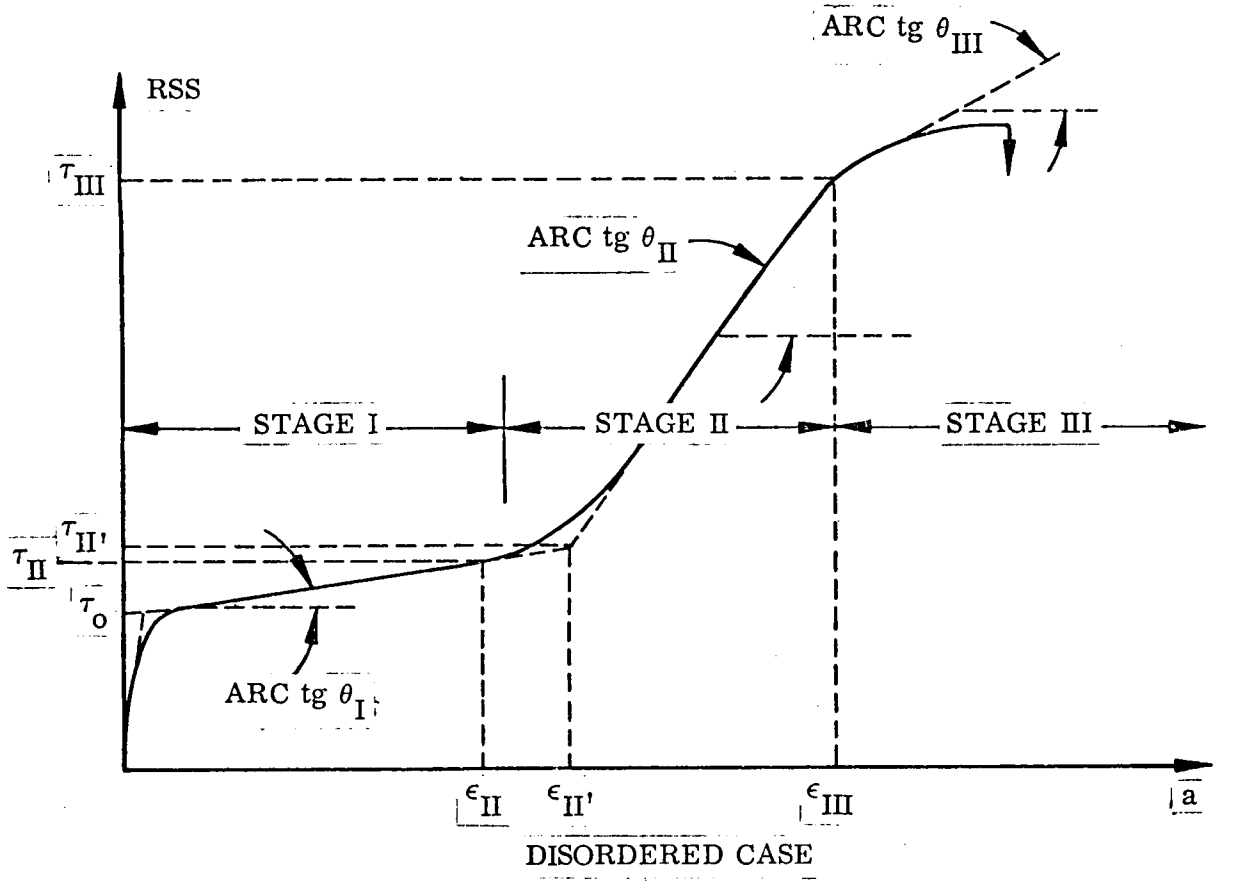

DISORDERED CASE

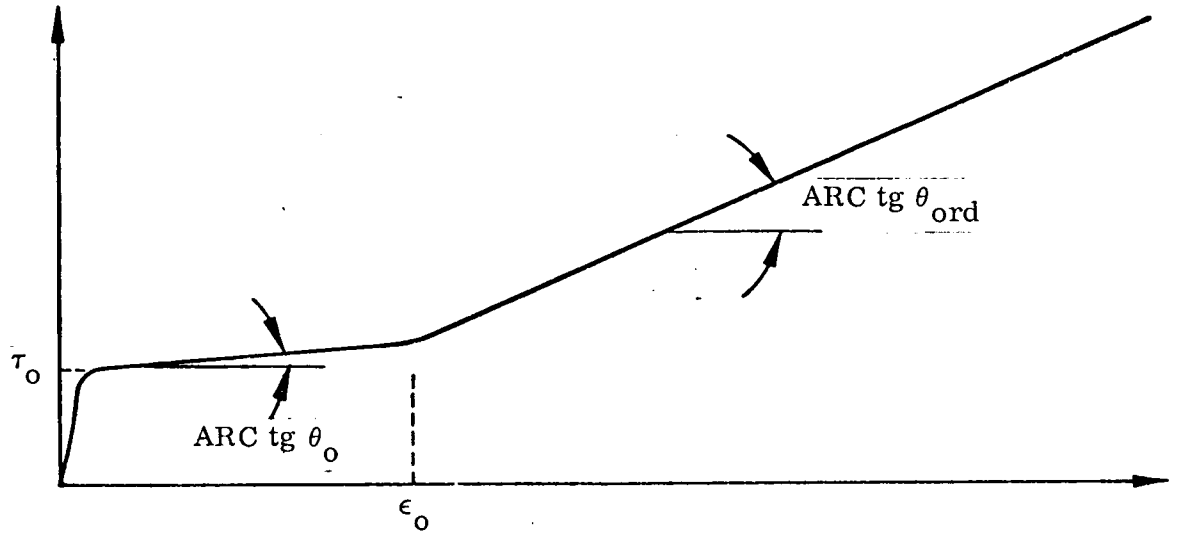

ORDERED CASE

Figure 10

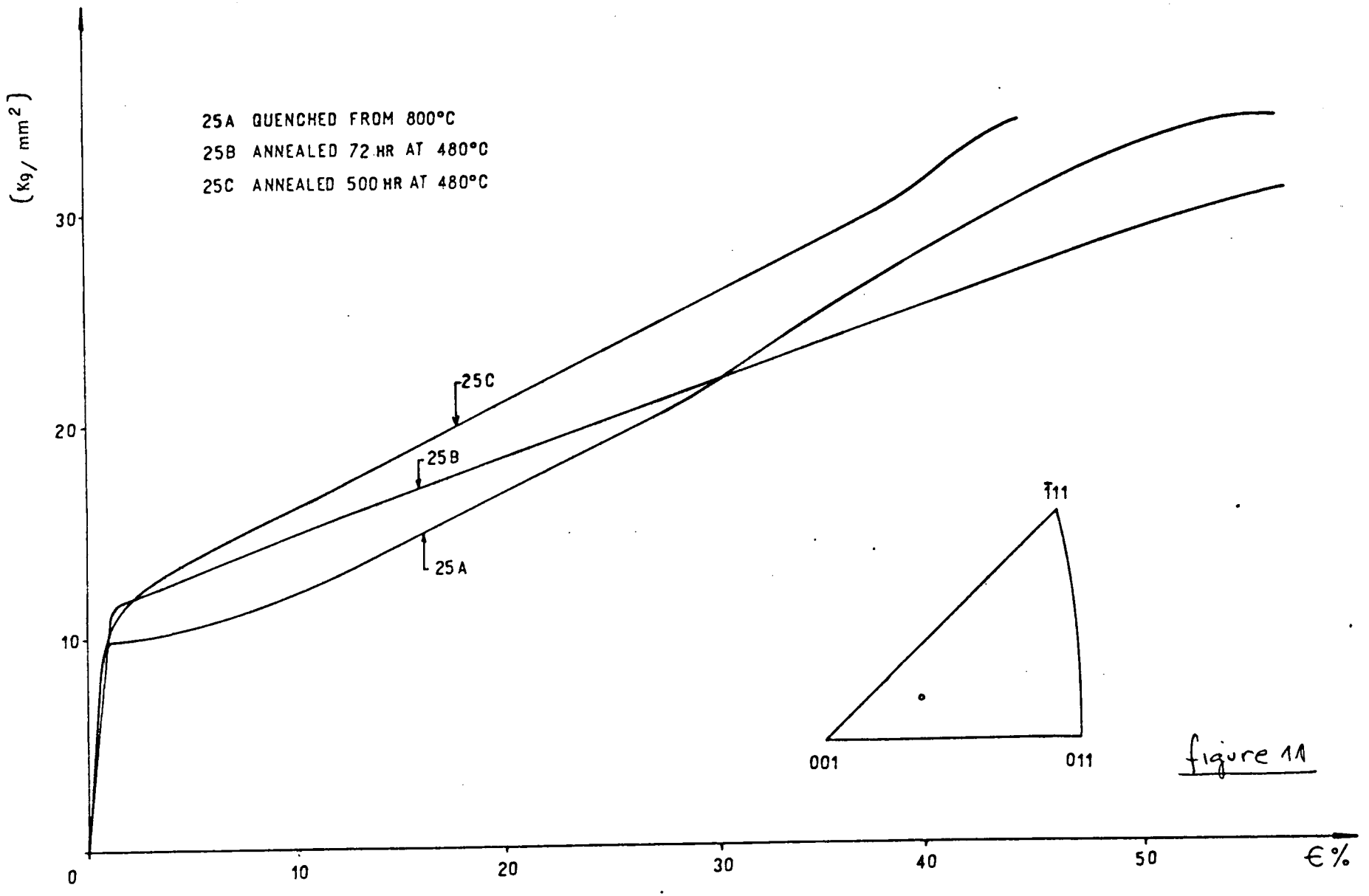
25A QUENCHED FROM 800°C
25B ANNEALED 72 HR AT 480°C
25C ANNEALED 500 HR AT 480°C
(kg/ mm²)
30
20
10
0
10
20
30
40
50
ε%
25C
25B
25A
111
001
011

figure 11

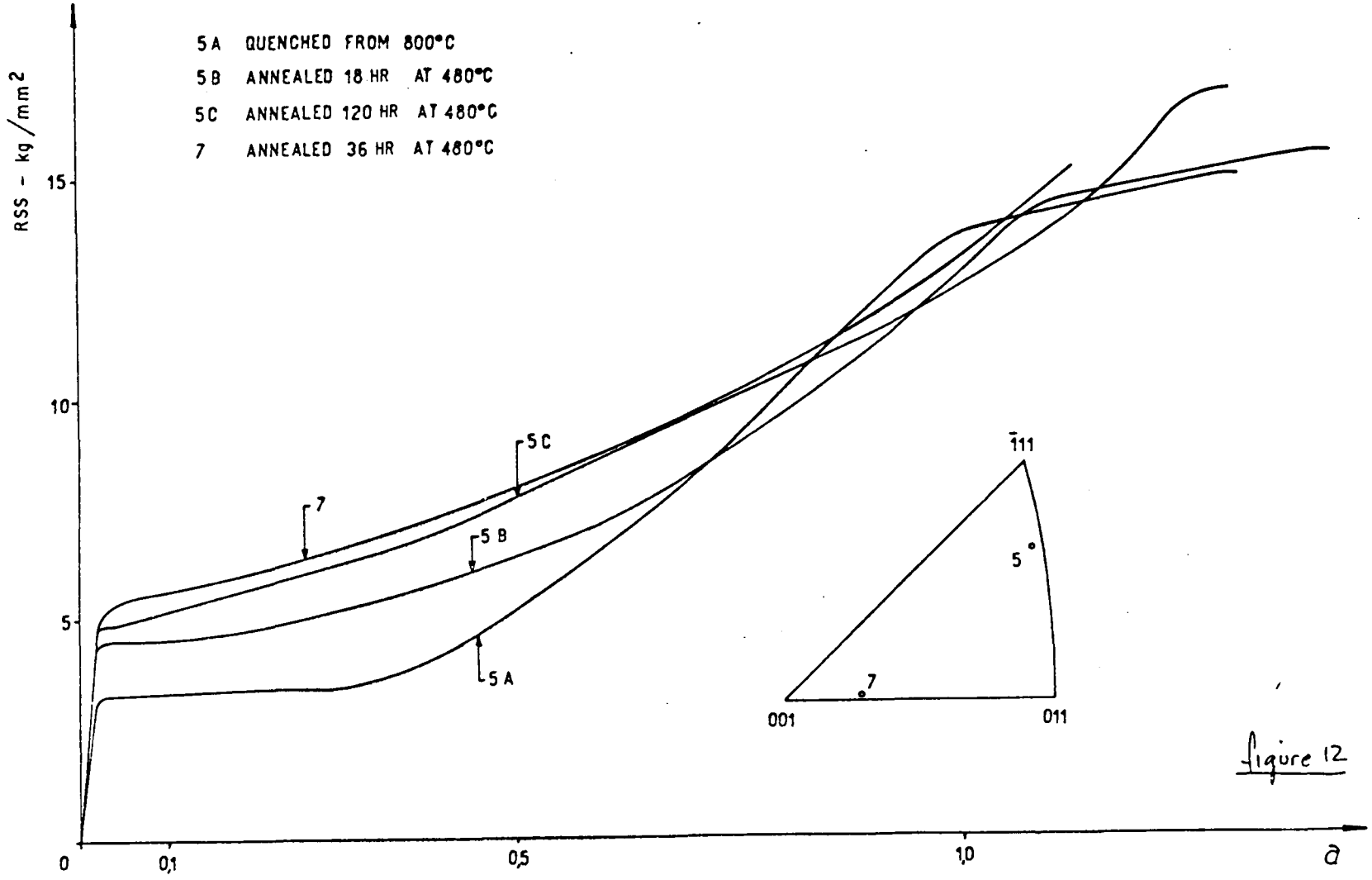
5 A QUENCHED FROM 800°C
5 B ANNEALED 18 HR AT 480°C
5 C ANNEALED 120 HR AT 480°C
7 ANNEALED 36 HR AT 480°C
RSS - kg/mm²
15
10
5
0
0,1
0,5
1,0
a
5 C
7
5 B
5 A
$\bar{1}11$
5°
7
001
011

figure 12

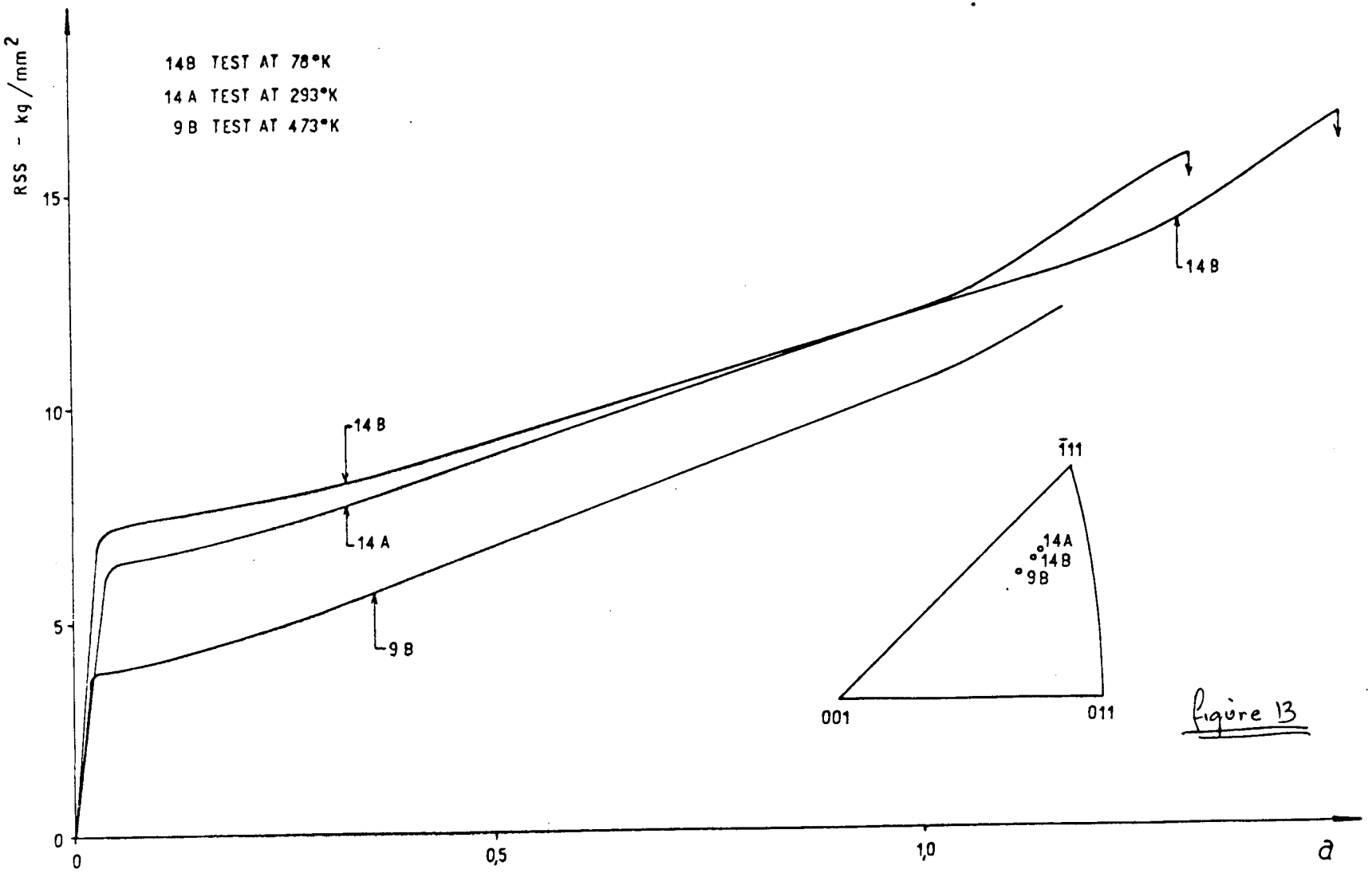
14B TEST AT 78°K
14 A TEST AT 293°K
9 B TEST AT 473°K
RSS - kg/mm²
15
10
5
0
0
0,5
1,0
a
14 B
14 A
9 B
14 B
$\bar{1}11$
14A
14B
9B
001
011

figure 13

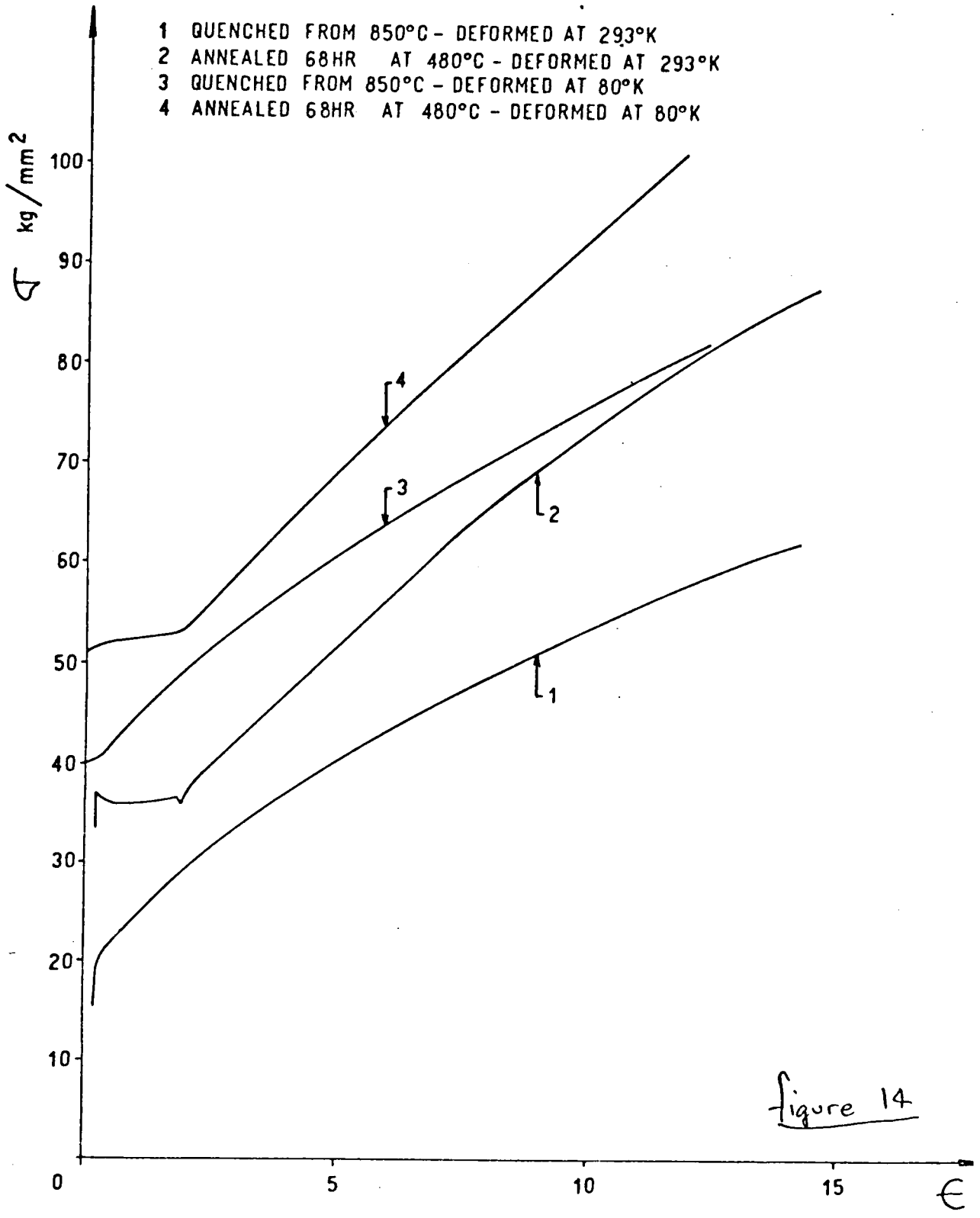
1 QUENCHED FROM 850°C - DEFORMED AT 293°K
2 ANNEALED 68HR AT 480°C - DEFORMED AT 293°K
3 QUENCHED FROM 850°C - DEFORMED AT 80°K
4 ANNEALED 68HR AT 480°C - DEFORMED AT 80°K
σ kg/mm²
100
90
80
70
60
50
40
30
20
10
0
5
10
15
ε
1
2
3
4

figure 14

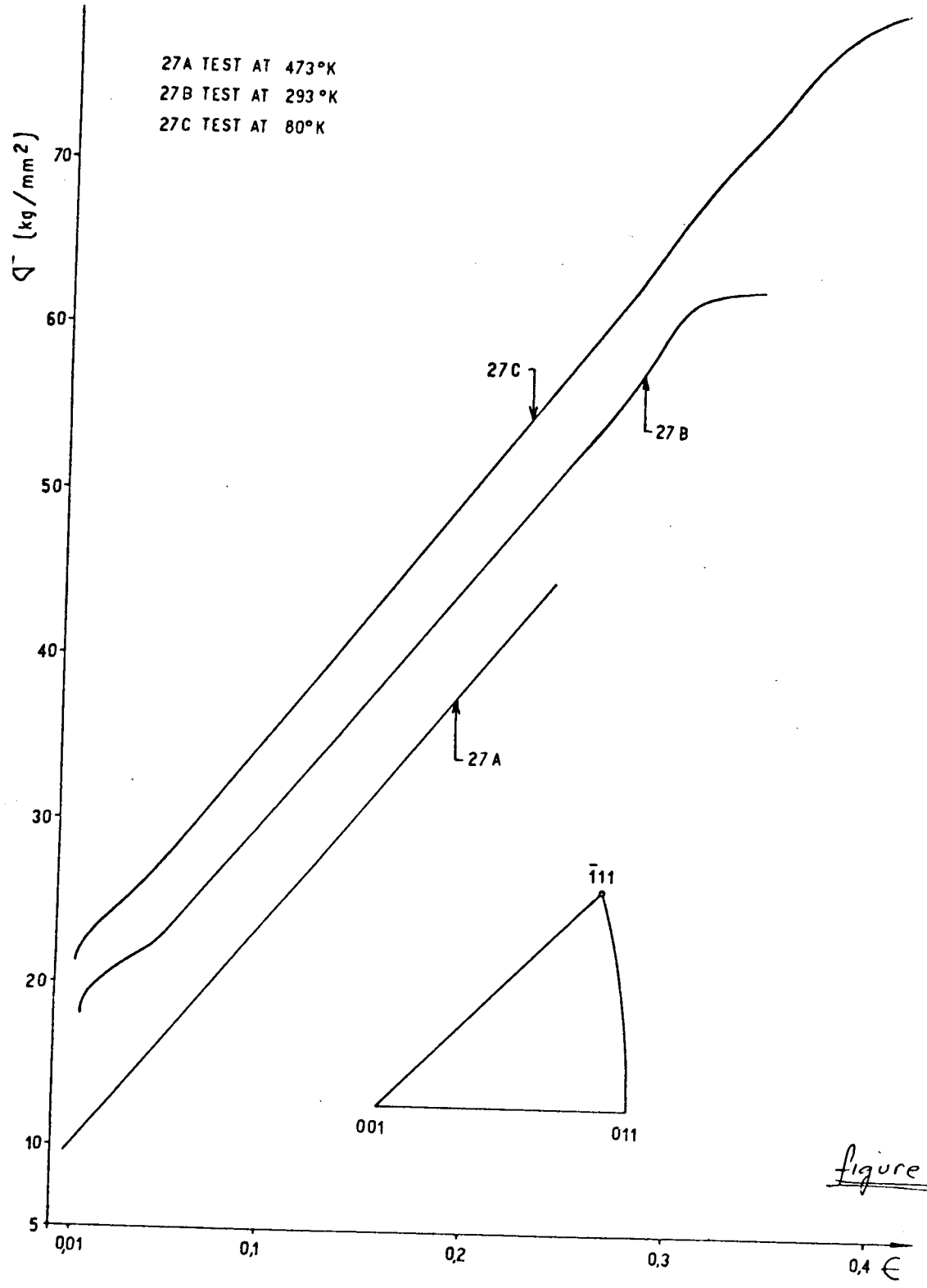
27A TEST AT 473°K
27B TEST AT 293°K
27C TEST AT 80°K
σ (kg/mm²)
70
60
50
40
30
20
10
5
0,01
0,1
0,2
0,3
0,4
ε
27C
27B
27A
111
001
011

figure 15

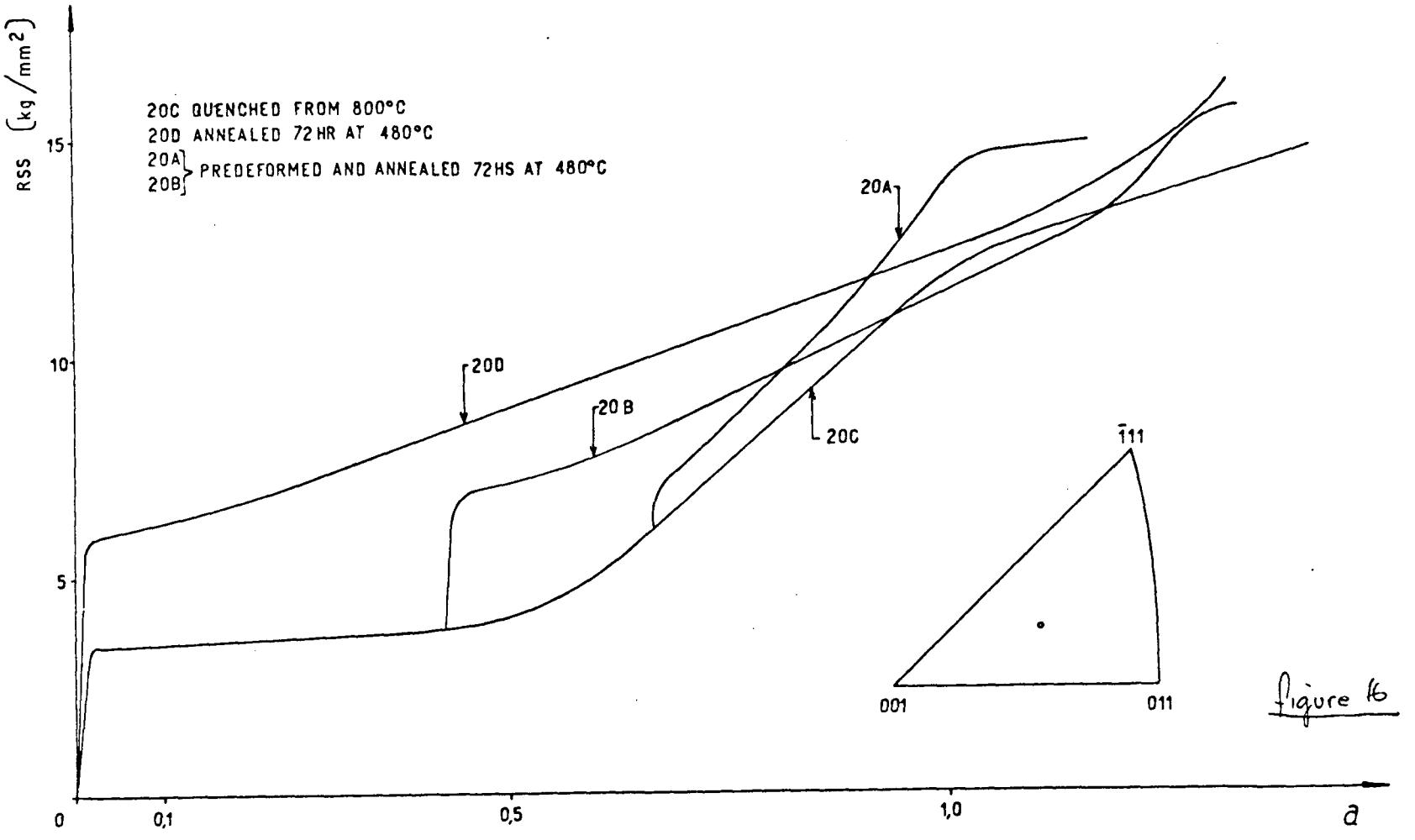
RSS (kg/mm²)
20C QUENCHED FROM 800°C
20D ANNEALED 72 HR AT 480°C
20A
20B
PREDEFORMED AND ANNEALED 72HS AT 480°C
20A
20D
20 B
20C
15
10
5
0
0,1
0,5
1,0
a
$\bar{1}11$
001
011

figure 16

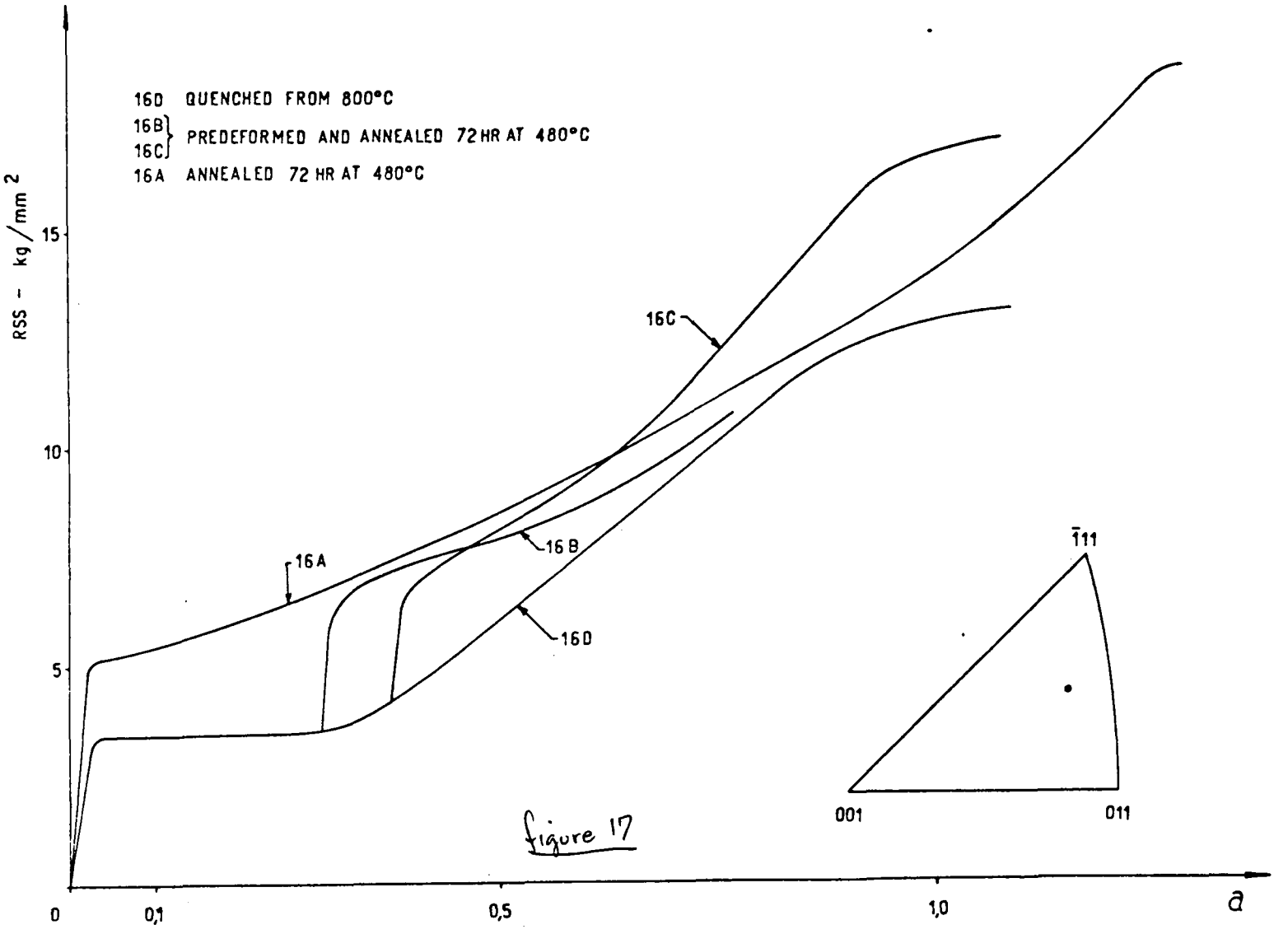
16D QUENCHED FROM 800°C
16B
16C
PREDEFORMED AND ANNEALED 72 HR AT 480°C
16A ANNEALED 72 HR AT 480°C
RSS - kg/mm 2
15
10
5
0
0,1
0,5
1,0
a
16C
16B
16A
16D
$\bar{1}11$
001
011

figure 17

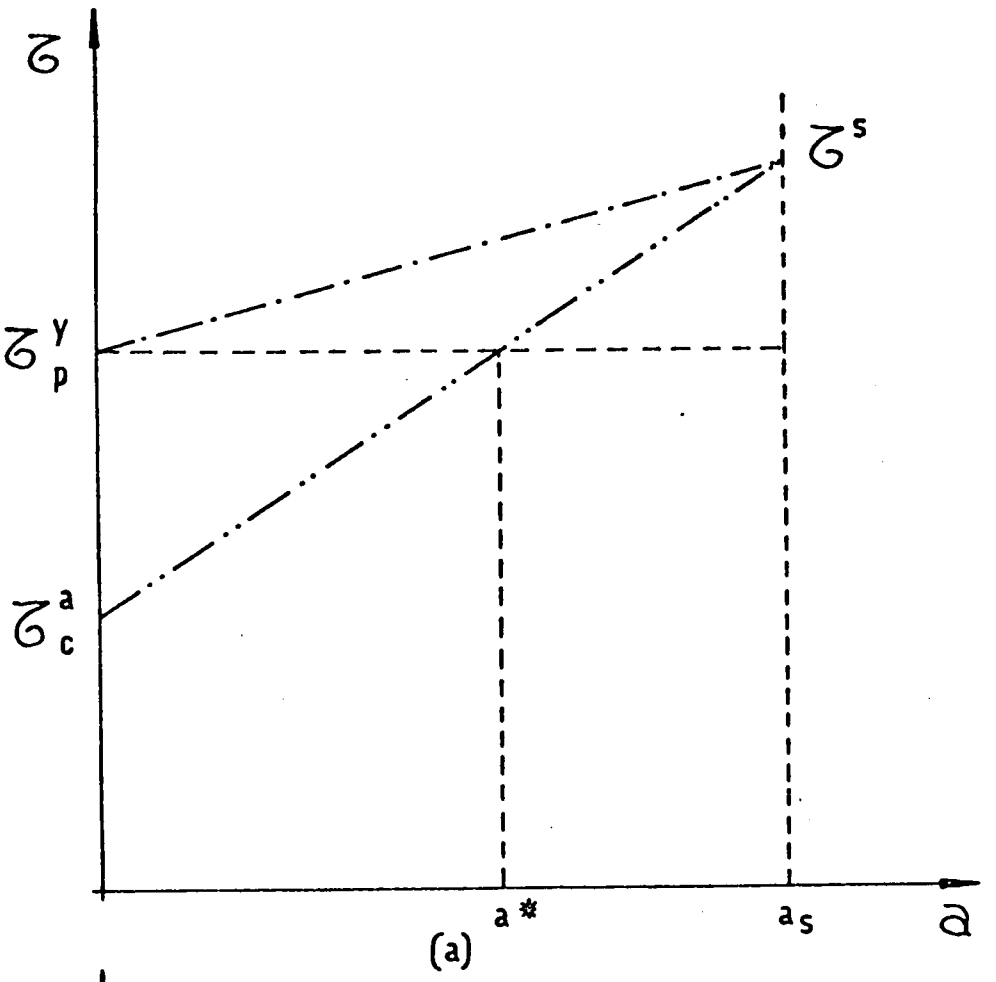
σ
σ^s
σ_p^y
σ_c^a
a*
a_s
a
(a)

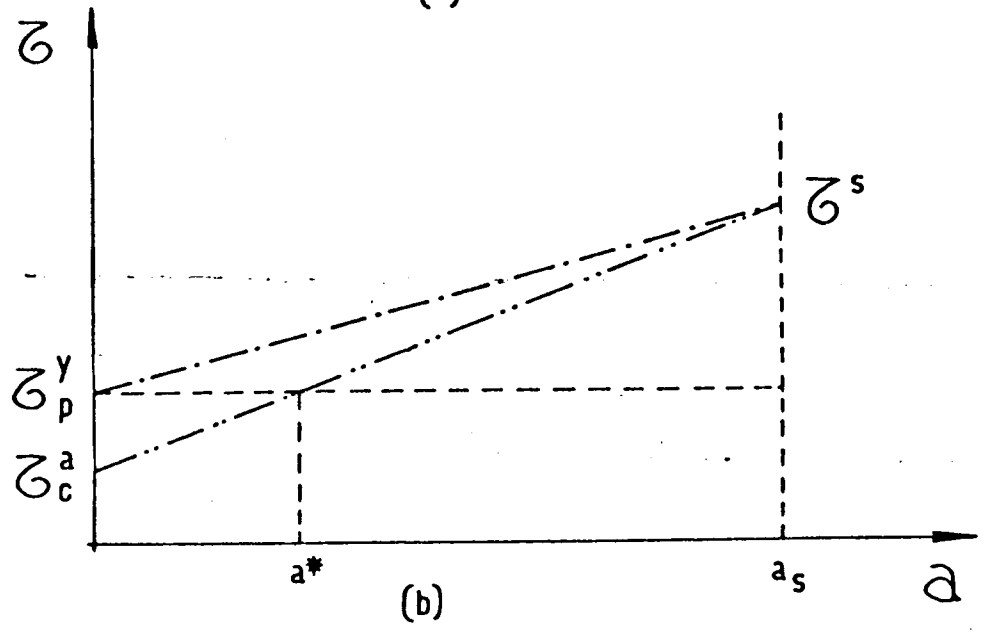
σ
σ^s
σ_p^y
σ_c^a
a*
a_s
a
(b)

figure 18